final report

Project code: A.TEC.0124

Prepared by: Jonathan Cook, Merv Shirazi
Scott Automation and Robotics
Graham Gardner
Murdoch University

Date published: 15 November 2016

PUBLISHED BY
Meat and Livestock Australia Limited
Locked Bag 1961
NORTH SYDNEY NSW 2059

X-Ray OCM Bone, Fat and Muscle Trials

Final Report

Meat & Livestock Australia acknowledges the matching funds provided by the Australian Government to support the research and development detailed in this publication.

This publication is published by Meat & Livestock Australia Limited ABN 39 081 678 364 (MLA). Care is taken to ensure the accuracy of the information contained in this publication. However MLA cannot accept responsibility for the accuracy or completeness of the information or opinions contained in the publication. You should make your own enquiries before making decisions concerning your interests. Reproduction in whole or in part of this publication is prohibited without prior written consent of MLA.

Abstract

An Automated Beef Rib Cutting system has been developed by Scott Automation & Robotics (SCOTT) and is currently in production. This system utilises dual-energy x-ray (DEXA) hardware to drive automated cutting of beef carcases. There is currently a need in the industry for methods to objectively measure carcase characteristics for the purposes of grading. DEXA technology is a key enabler for this.

The purpose of this project was to investigate the ability of this system to accurately perform objective carcase measurement (OCM) on beef sides for fat, lean and bone composition. A trial was first performed using a calibration object made from known compositions of fat and lean. These trials suggested that the system was capable of obtaining OCM data. A set of trials was then performed whereby six beef sides were scanned by the DEXA system and then by a CT scanner. From this, the DEXA images were analysed and models were built to predict the amount of lean, fat and bone present in each DEXA image. The CT data provided predictions for the amount of lean, fat and bone in each carcase side.

These trials yielded promising results and a second set of trials was designed to build upon these findings. Another set of phantom trials were performed and a further eight sides were then scanned by the DEXA system, CT scanned and modelled as before. The modifications resulted in improved models with R^2 values of 0.78 and 0.93 achieved for fat and bone, respectively. Alternatively there was no ability to predict CT lean% directly, although this can be calculated from the other two measures.

This data demonstrates good potential for measuring carcase composition using DEXA values. The next phase of work should involve confirming these results within an expanded data set, while also testing the stability of this measurement across a variety of processing factors.

Executive Summary

An Automated Beef Rib Cutting system has been developed by Scott Automation & Robotics (SCOTT) which is currently in production in an Australian beef abattoir. The system utilises a dual-energy x-ray (DEXA) system in order to identify cut placement for that carcase. This system consists of separate source-detector pairs for each of the low-energy and high-energy x-ray images. These two images are then stitched together into one DEXA image.

There is a need in the red meat industry to move towards methods of measuring carcase attributes in an objective manner. DEXA is one technological enabler for such measurement. Utilising DEXA technology for both automation and OCM concurrently, in one integrated system, presents a number of benefits, particularly surrounding the cost-benefit of such a system.

This project thus aimed to evaluate the feasibility in utilising a system which has been designed and built for beef automation for OCM tasks as well. It will also explore the hardware requirements and commercial considerations for designing such systems in the future as well as the suitability of dual-hardware DEXA systems for the application.

The first task was to get an initial assessment of whether the hardware was capable of producing consistent values for OCM measurements. This was achieved by scanning a tissue phantom – an object consisting of homogenous blocks of lean and fat, at varying compositions, which have been tested for chemical lean. The scans were completed successfully and analysis suggested the system was capable of producing consistent enough x-ray values to enable OCM calculation.

Six beef sides were then selected and scanned with the system. These sides were then cut up and scanned with a CT scanner. The CT data was then used to predict the amount of fat, lean and bone in each of the sides. The DEXA images were analysed to see if the information could be modelled to predict CT composition. A number of challenges were experienced however which prevented an accurate model to be generated. One factor contributing to this was an effect along the height of the detector. The detectors in the system are 2500mm long and thus have significantly different x-ray flux along their lengths. Compensating for this improved results significantly. Another effect found was that thin tissue information (approximately 10mm and less) was saturated in the low energy image. In the work completed in lamb, these tissue depths are known to contribute significantly to the OCM models. The loss of such information thus impacted the results negatively.

Another set of trials was then conducted whereby scans were taken at production currents as well as a current low enough to avoid saturation of the detectors. Phantom scans were first performed which vindicated the positive effect of running at these lower currents – the information in the thinnest phantom were now visible and demonstrating consistent results. Another eight sides were then DEXA scanned, CT scanned and analysed.

The results of the analysis on the additional eight sides yielded better results, particularly for predicting bone content. Fat and lean content however were unable to be modelled with a significant level of accuracy. R^2 values of 0.4, 0.45 and 0.82 achieved for lean, fat and bone, respectively. A number of possible limitations have been identified which may explain why this system is not able to achieve accurate OCM. It is suspected that the alignment

between the low energy and high energy pixels, while sufficient for the purposes of cutting, aren't sufficient enough to allow accurate OCM analysis. The other key limitation is that the x-ray system doesn't scan the entire carcase – it was only designed to image the carcase ribs and, thus, doesn't capture the hindquarter. Finally, while scanning at a lower current enabled more accurate OCM measurements, it also negatively affects the system's ability to perform cutting.

A second analysis was then performed whereby the image the was truncated at the 13th rib for each of the carcases. This ensured that all datasets contained the same carcase information (the forequarter only). In this case the prediction of CT bone composition was excellent, with R2 values as high as 0.78, and 0.93 when cold carcase weight was included in the model. There was also good precision for CT fat% prediction with R2 values as high as 0.71, and 0.78 when cold carcase weight was included in the model. Alternatively there was no ability to predict CT lean% directly, although this can be calculated from the other two measures.

This data demonstrates good potential for measuring carcase composition using DEXA values. The next phase of work should involve confirming these results within an expanded data set, while also testing the stability of this measurement across a variety of processing factors.

Table of Contents

1 Background

Scott Automation & Robotics (SCOTT) has developed an Automated Beef Rib Cutting machine using dual energy x-ray (DEXA) technology to determine cutting lines. The purpose of this project is to determine whether the same x-ray technology can deliver Objective Carcase Measurement (OCM) of bone, fat and muscle.

SCOTT will utilise the x-ray technology present in this system to perform preliminary offline trials, analysing beef primal cuts and portions to determine whether the technology can deliver OCM of bone, fat and muscle composition. Murdoch University will be engaged to develop the trialling methodology, assist in conducting the trials and to perform the analysis required to assess whether the Automated Rib Cutting x-ray system is suitable for beef OCM calculations.

Below are examples of the images SCOTT has successfully obtained in their x-ray Rib Cutting project:

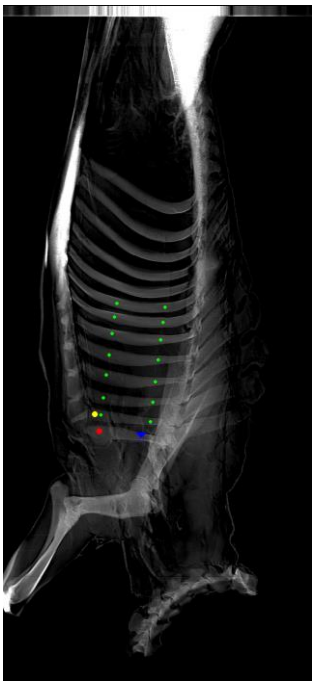

Identifying sensing technologies able to improve current processing and/or provide a platform for OCM and automation is a key focus for automation RD&E suppliers such as SCOTT and the industry as a whole. Currently, there is no single technology proven to be able to measure carcase OCM characteristics while also being able to enhance or provide a platform for automation, particularly for beef processing. Being able to utilise a single x-ray system as a platform for Automation and OCM will provide a major step in sensing automation for red meat processing.

Potential benefits of successfully advancing the use of pre-developed technology for OCM includes:

- Utilisation of common technology for OCM and automated cutting (cost, footprint, enhanced return on investment)

- Ensuring maximum meat and economic yield from each and every carcase
- The ability to better meet customer/market requirements
- Automated grading and carcase assessment
- The ability to influence livestock quality and price
- Beef Rib Cutting using existing x-ray system installed for automated cutting production

An additional expected outcome of successful OCM trials is to enable and assist future development strategies for process automation with a view of establishing a considered strategy for future R&D project investment.

Existing and new automated cutting systems developments would benefit immediately if successful by implementing OCM together with automated cut line detection in a single x-ray system.

A path to industry adoption could be tested on existing SCOTT developments.

2 Project Objectives

An Automated Beef Rib Cutting system has been installed and is in production at an Australian beef-processing facility. The system contains two x-ray tubes and two separate x-ray detectors located adjacent to each other on a conveyor system. The principal role of this system is to meet the imaging requirements of the automated rib cutting system utilised by this plant. However, its potential for determining carcase composition requires investigation.

The project will provide the following outcome:

- Confirm whether the dual energy x-ray technology used in SCOTT's Beef Rib Cutting Project can be used to provide Objective Carcase Measurement of Bone, Fat and Muscle in beef primal cuts and portions.

A Final Report including videos, images, results and outlining challenges and success in achieving project goals and outlining any future development steps to be submitted to MLA for review and approval.

3 Methodology

3.1 DEXA Scans of Tissue Phantoms

Samples of lean and fat tissue were sourced from lamb carcases and used to create mixtures of the following fat:muscle ratio's: 0:100, 25:75, 50:50, 75:25, or 100:0. These samples were then ground and homogenised, after which subsamples were taken for the determination of chemical fat and lean percentage, and percent dry matter, as reported in **Error! Reference source not found.** below.

Table 1. Dry matter, chemical fat and chemical lean percentage of mixtures of fat and lean.

Fat:Lean ratio	Percent Dry Matter	Chemical Fat %	Chemical Lean %
100:0	26.6	88.0	12.0
75:25	36.3	60.6	39.4
50:50	53.4	40.0	60.0
25:75	70.2	18.3	81.7
0:100	91.4	6.2	93.8

These mixtures were then used to create calibration blocks of 3 different uniform sizes using custom built moulds which were 10mm, 80mm, or 160mm thick. Thus 3 calibration blocks were created for each of the 5 fat:lean mixtures, with thicknesses of 10mm, 80mm, or 160mm. X-Ray images were then generated of the phantoms. This entire process was repeated 3 times using 3 sets of 3 calibration blocks.

Prior to carrying out image analysis, sections within each image were selected which corresponded to the calibration tissue. The corresponding pixels within the low and high energy images were then used to calculate an R-value for these pixels according to the following formula:

$$(R = \ln(I_{Low}/Air_{Atten}) / \ln(I_{High}/Air_{Atten}));$$

Where: I_{Low} represents the pixel value in the low energy image (ZnSe Photodiode)
I_{High} represents the pixel value in the high energy image (CsI Photodiode)
Air_{Atten} represents the pixel value corresponding to the un-attenuated photons (I_0) in the white part of each image.

Equation 1 - R-value calculation

The R-values for the pixels of each calibration block were then averaged to give a single R Value representing that block. This data was represented graphically relative to the corresponding chemical fat % for that block.

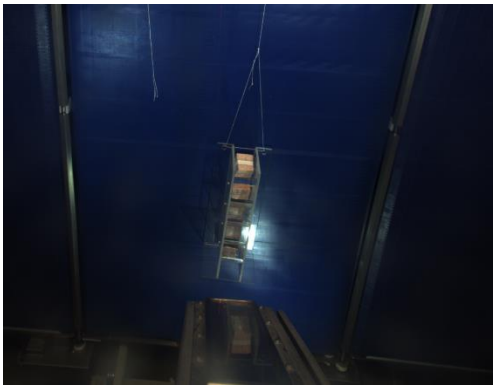

Figure 1: Dynamic DEXA scanning - Carcass phantom mid scan

Figure 1 above is a snapshot of the carcass phantom as it is being scanned. The five blocks that can be seen are each various combinations of meat/fat/bone compositions and thicknesses. Each block had to be rearranged from various “slides” of meat/fat/bone for every scan.

Figure 2 below depicts partially processed images of two different “carcass phantom” configurations. It can be seen that each tile is a slightly different shade and this corresponds to the fat, meat and bone composition of each tile.

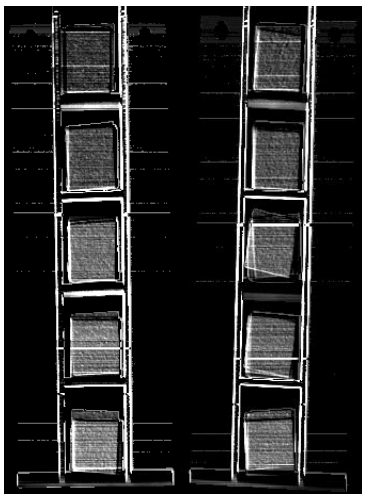

Figure 2: Dynamic DEXA scans of two carcass phantoms

3.2 DEXA and CT scanning of six beef sides

The DEXA hardware at the beef processing plant was used to capture dual energy images of 6 beef half- carcases, scanned in 2 batches of 4 (batch 1), and 2 (batch 2) carcases, with each batch collected on separate days. The DEXA hardware consisted of two X-ray tubes (one operating at high voltage and one operating at low voltage) and two GADOX photodiodes located at separate points along a conveyor used to maintain carcass orientation. These two x-ray tube/detector combinations produce the high and low energy images which are then used to calculate an R-value for these pixels according to Equation 1.

The average R-value for all of the pixels in the carcase image was calculated, and the image was then reconstructed after removing any pixels with R-values lying above this mean R-value. Pixel R-values were then converted to proportion lean tissue and weighted based on thickness using the equations derived in the section above, and then averaged to reflect an average R-value for the whole carcase. These carcase R-values were then used to predict CT lean%, fat%, and bone% measured on these same carcases.

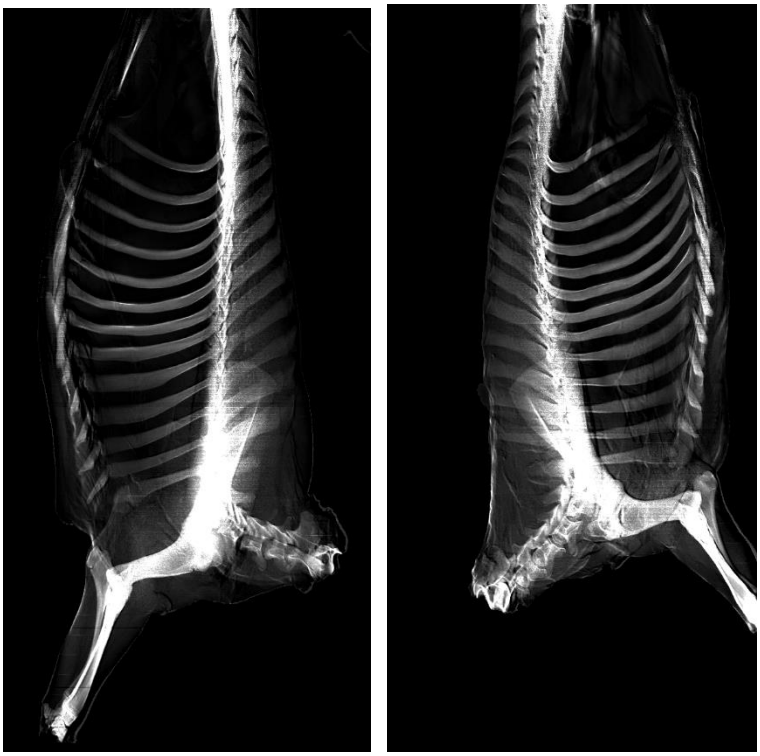

Figure 3: DEXA scans of two carcass sides

The beef carcasses that were DEXA scanned were broken down into primals, vacuum packed and sent to a CT scanner. The CT scanning of 53 cartons of product to determine lean meat, fat and bone composition and distribution was successfully completed. Full bone out was conducted so that manual objective measurements could be taken.

Figure 4 shows a series of images of the vacuum packed “primals” being scanned.

Figure 4: Vacuum packed "primals" being CT scanned

Figure 5 shows a number of the topographical outputs from the CT scans. They provide an overhead view of the scanned primals.

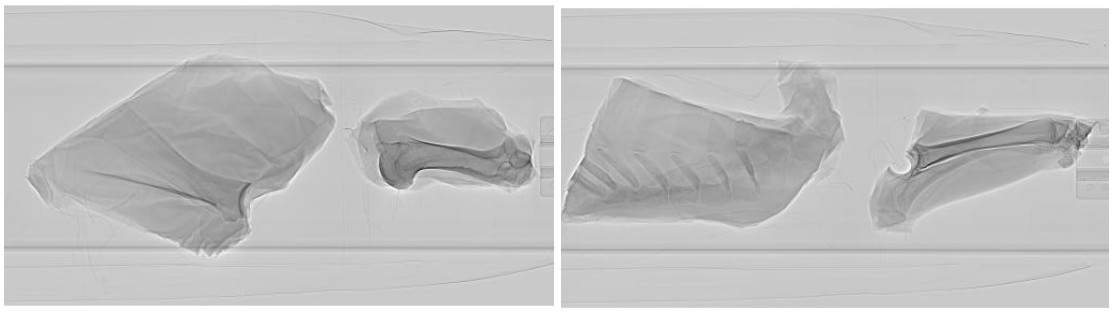

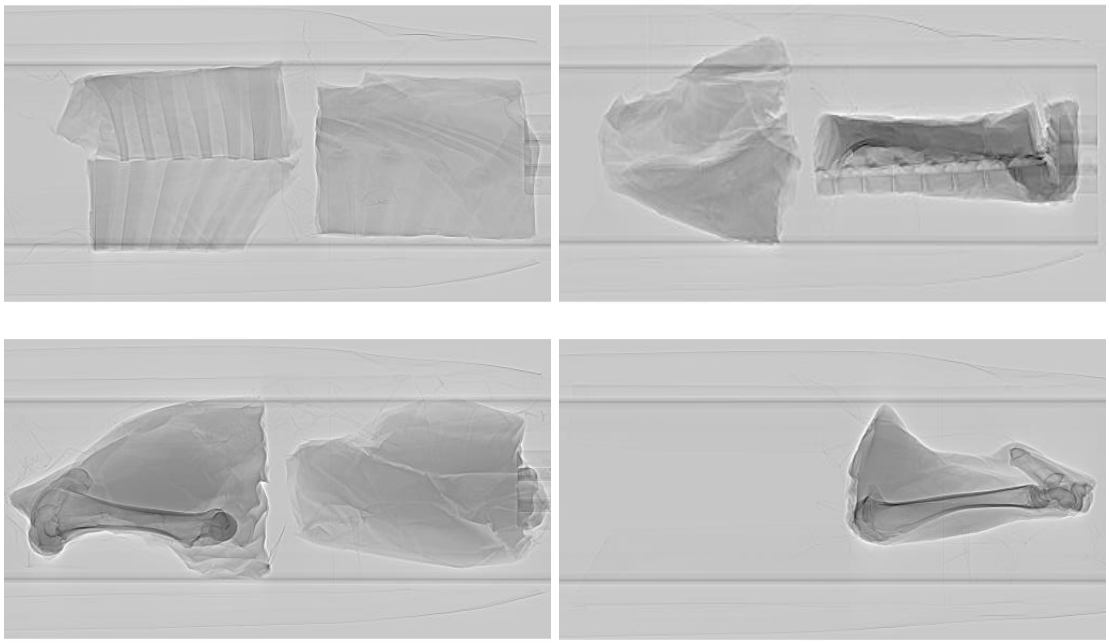

Figure 5: Topographic images of beef primals

Figure 6 shows examples of the slice images from the CT machine. They represent the density distribution across a single cross-sectional slice of a primal. Each scan will result in many hundreds of slice images which, when combined and processed, represent the full primal in 3D.

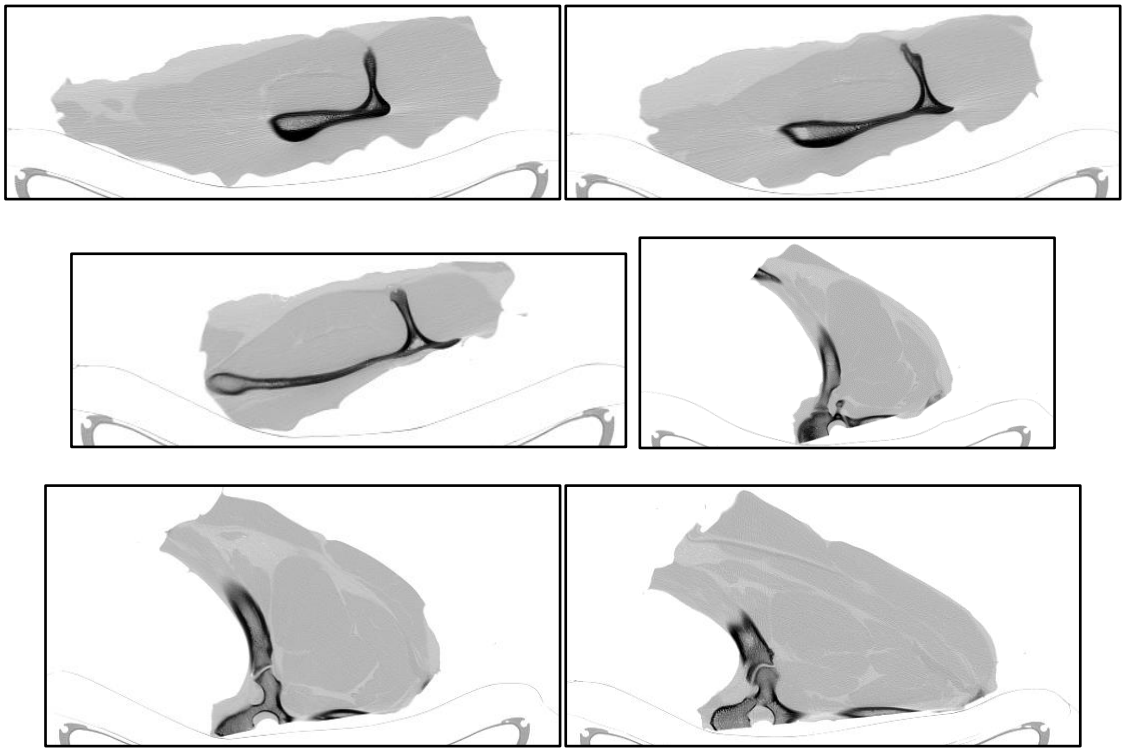

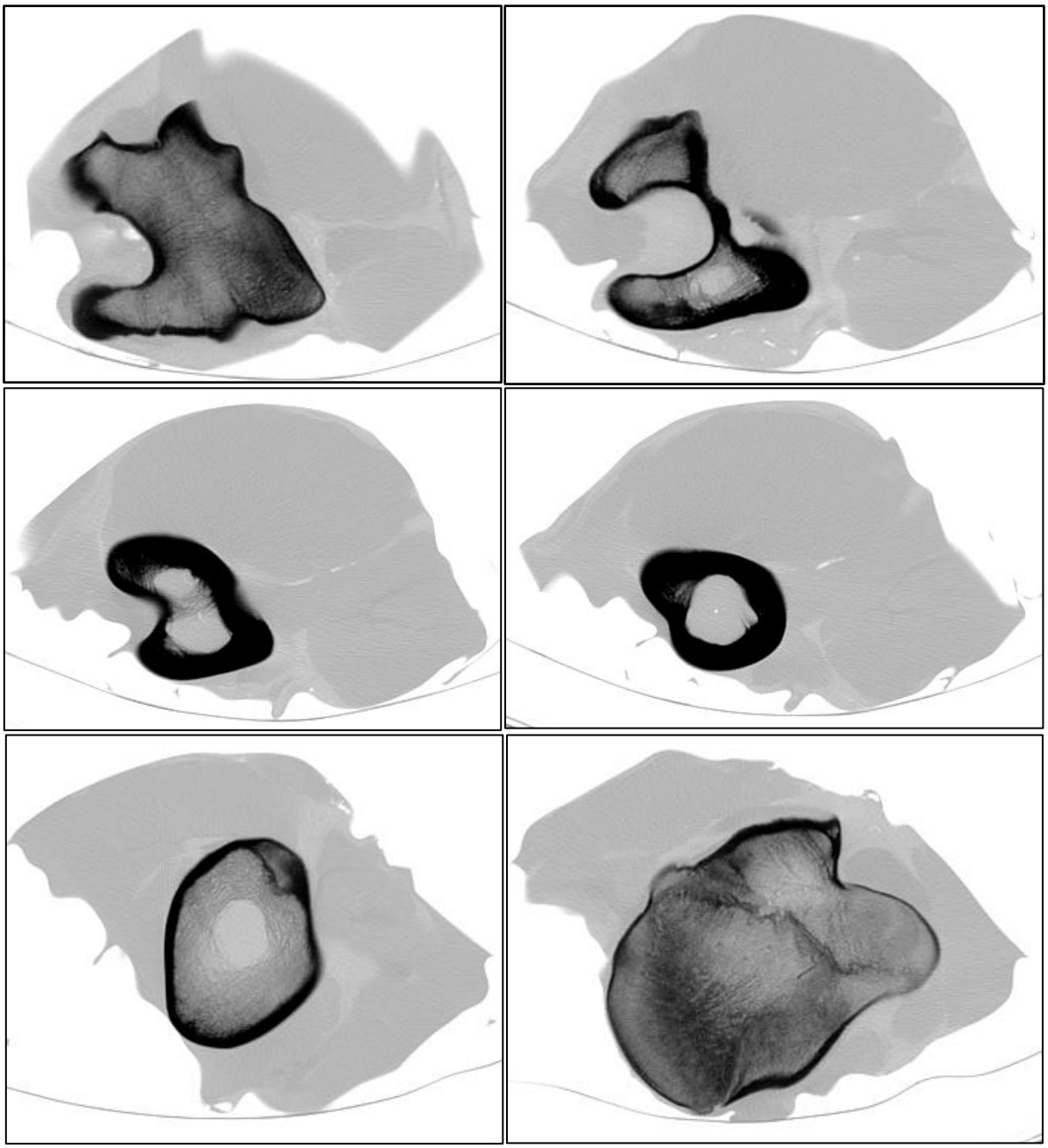

Figure 6: Slice images of beef primals

3.3 Second set of phantom and carcase scans at production X-Ray levels and reduced X-Ray levels.

Initial analyses performed on the data obtained for the six beef sides evaluated through the dual-hardware DEXA setup indicated that the system demonstrates good potential for beef fat:lean ratio. During this analysis, a number of opportunity areas were also identified which may help to improve upon the result obtained. Thus, it was decided to perform another set of trials to gain a greater understanding of the behaviour of the system in the context of OCM and to achieve a higher level of confidence in the assessment of whether accurate OCM can be achieved with the system in its current configuration.

A second set of trials was designed to build upon this knowledge to further characterise the OCM capabilities of the Automated Beef Rib Cutter's x-ray system. This involved performing another set of phantom trials and scanning a further eight beef sides. The trial design was thus to:

- Take scans at production X-Ray settings as well as reduced current to allow visibility of 10mm tissue depths
- Rescan the phantoms at these lower energy levels and at different heights along the detector
- Scan another 8 sides – 2 heavy, fat; 2 light, fat; 2 heavy, lean; 2 light, lean
- Break down sides into primals, and scan with the CT scanner.

Figure 7: Scans of phantoms – colour image, high energy and low energy images at reduced X-Ray settings

Once the phantom scans had been performed, eight sides were selected which were each scanned. As part of these trials, the following scanning protocol was used for each side:

- Phantom at reduced X-Ray settings
- Phantom at production X-Ray settings
- Carcase side at production X-Ray settings
- Carcase side at reduced X-Ray settings

The carcase data for the sides selected for the trial is shown in Table 2.

Table 2: Trial Carcase Data

Carcase ID	Weight	Fat Depth
901R	117.5 kg	8mm
908L	129.0 kg	4mm
926R	138.0 kg	3mm
954L	131.0 kg	12mm
1259L	118.5 kg	18mm
1268R	115.0 kg	5mm
1270L	114.5 kg	6mm
1272R	131.5 kg	13mm

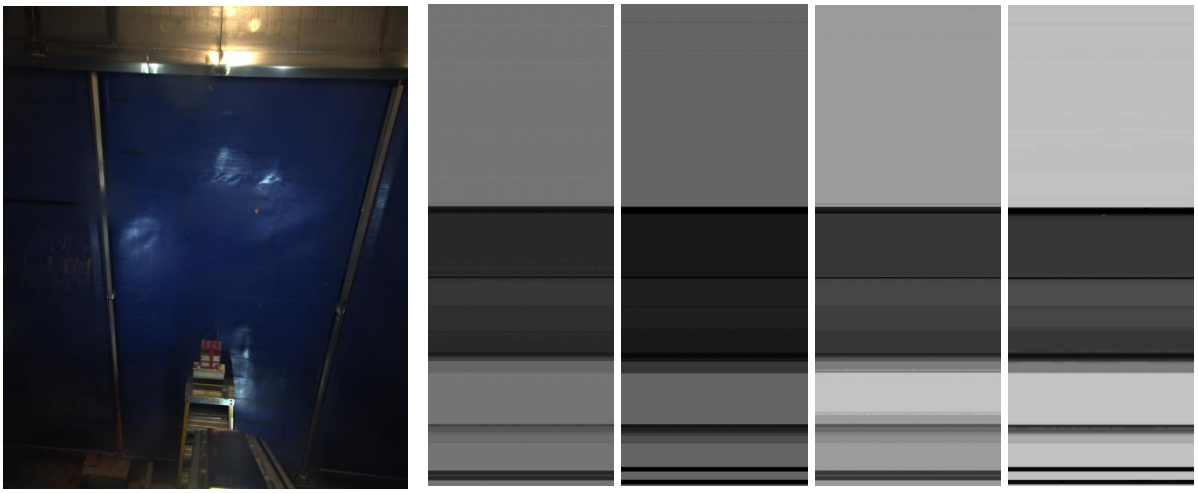

Figure 8: Phantom Scans – (Left to Right) Reduced X-Ray settings (high energy, low energy), Production X-Ray settings (high energy, low energy)

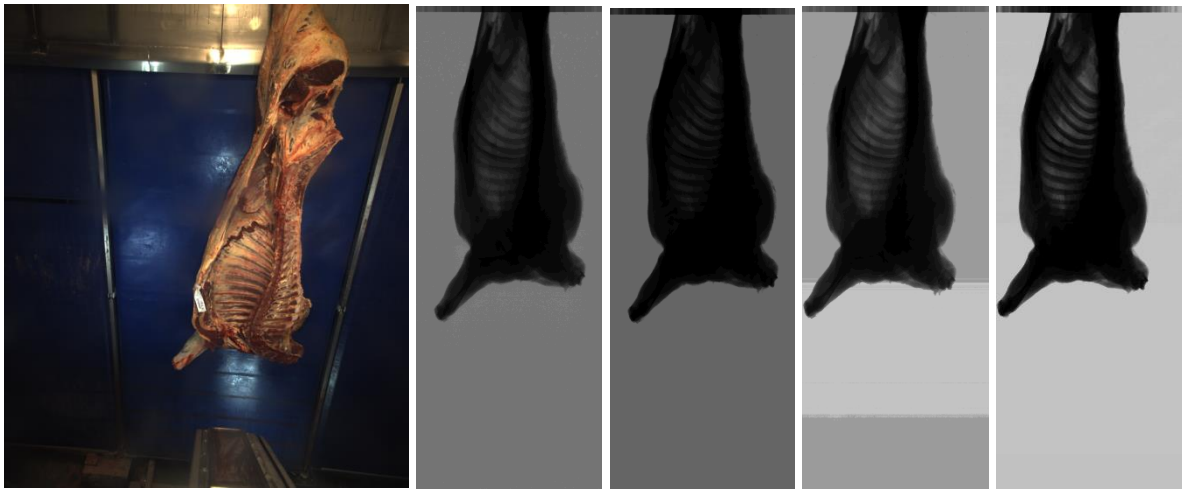

Figure 9: Carcase scans – (Left to Right) Reduced X-Ray settings (high energy, low energy), Production X-Ray settings (high energy, low energy)

The carcase sides were then cut into primals and scanned with the CT scanner. The carcase sides were broken down into the following primals for scanning:

Forequarter

- Fore shank, Bolar
- Naval End Brisket
- Point End Brisket
- Ribset
- Rib Plate
- Chuck
- Chuck Rib
- Neck
- Blade

Hindquarter

- Hind Shank
- Topside, Silverside, Femur
- Knuckle
- Rump
- Loin
- Flap

With the data acquisition completed, the data analysis was undertaken by Murdoch University.

4 Results/Discussion

4.1 DEXA Scans of Tissue Phantoms

There was a negative linear relationship between increasing chemical fat % and the corresponding average R value for the 80 mm and 160 mm tissue phantoms (Figure 10). Thus in the 80 mm tissue phantom increasing chemical fat % from 6.2 up to 88% decreased the average R Value by about 0.15 units (from 1.12 down to 0.97). However, the sensitivity of this relationship diminished as the calibration block thickness increased such that for the 160 mm tissue phantoms, the average R values only decreased by 0.11 units across the same increasing chemical fat range.

Therefore, the DEXA system loses sensitivity for determining fat:lean composition when passing through tissues of greater depth. A similar result was evident in the tissue phantom scans using the border town DEXA system.

No calculations were possible from the 10 mm tissue phantoms as these were not visible within the low energy image. This is due to the x-ray levels currently being used saturating the detector at these low tissue thicknesses. This implies that tissue depths of less than 10 mm (and possibly higher) within carcass images would not have been detected. Although difficult to discern from Figure 11, upon close inspection it was found that the low energy images were in fact missing the outer pixels detected on the high energy images. This is cause for concern as it is likely that these thin tissue regions have significant prediction power for determining carcass composition.

The other striking attribute of all images collected was the differential background attenuation evident within the high energy images. This is clearly evident within Figure 11, with the yellow shaded background having pixel values in the order of 4000 as opposed to the green shaded background which had pixel values in the order of 8000. This background artefact did not appear to impact upon the pixel values of the carcass or phantom tissues themselves, which were quite consistent across all regions of the image. For calculation purposes pixel values in the order of 8000 were chosen as the un-attenuated values used in the R-value formula described in Equation 1.

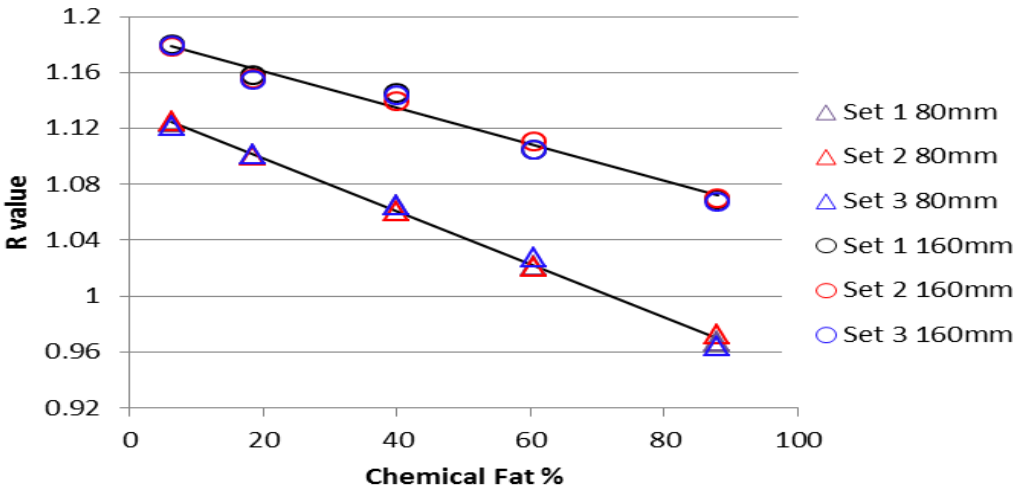

Figure 10: Relationship between R value and chemical fat % in tissue calibration blocks of 80mm, and 160mm.

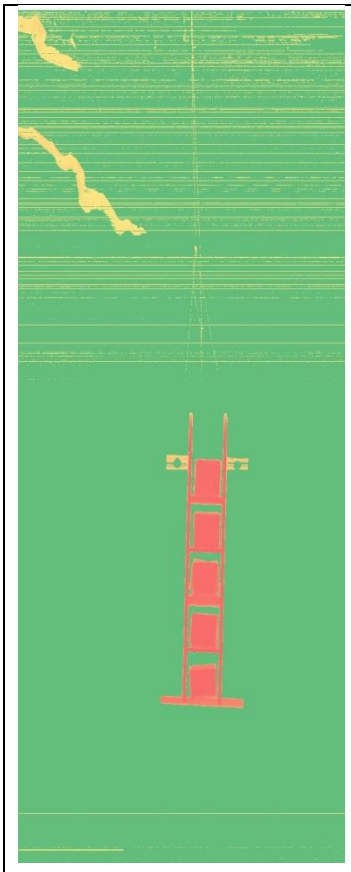

Phantom Low Energy

Carcase 1 Low Energy

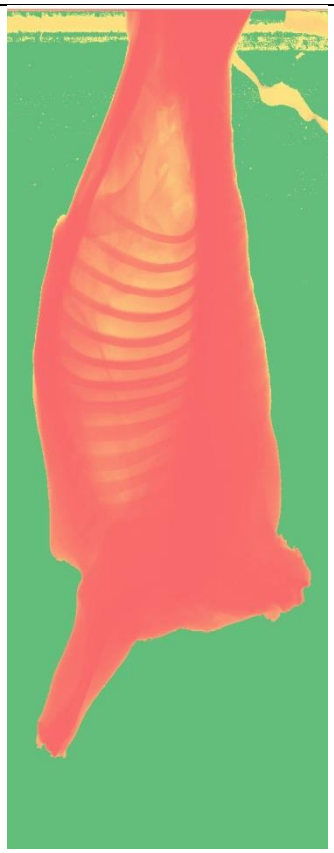

Carcase 4 Low Energy

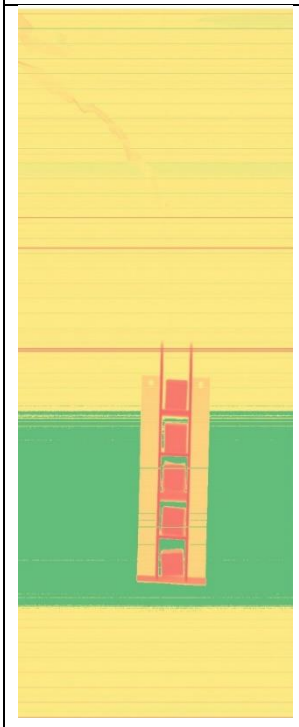

Phantom High Energy

Carcase 1 High Energy

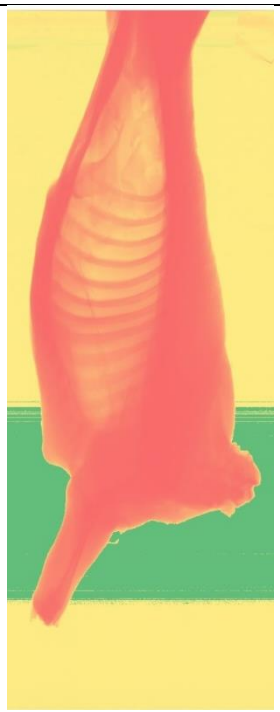

Carcase 4 High Energy

Figure 11: DEXA images of 80mm tissue phantom block, carcase 1 and carcase 4.

When this relationship is inverted and a general linear model is used to describe percent lean it has a high degree of precision (98.9% of variance described), with the coefficients as shown in Table 3**Error! Reference source not found.**. This implies that we can solve for Chemical Lean % but must have knowledge of both R-values and tissue thickness.

Table 3: F-values and coefficients for the prediction of chemical lean % using average R-value and thickness of calibration blocks.

	Percent Lean	
	F value	*Coeff±SE*
Intercept		-211.1±40.35
R value	68.01*	307.3±37.26
Thickness	96.71*	-3.59±0.366
*R value*Thickness*	69.08*	2.74±0.330
R-Square		0.989
RMSE		3.262

*, P<0.01; Thickness = tissue thickness (mm); RMSE, Root Mean Square Error.

Therefore the potential for determining tissue thickness by using the log(pixel value) from the low energy image was further investigated. When assessed graphically, the relationship between tissue thickness and log(pixel value) demonstrated a linear trend (Figure 12**Error! Reference source not found.**), with the 200mm calibration blocks having log(pixel values approximately 3.5 units lower than the 10mm calibration blocks.

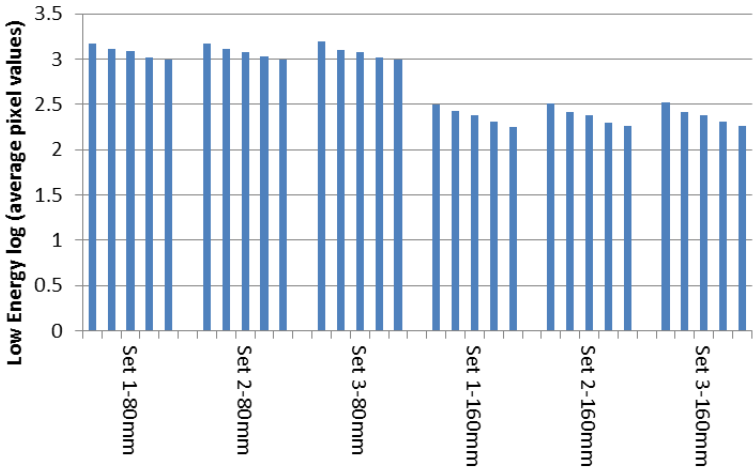

Figure 12: Log(average pixel value) from the low energy image for each of the calibration blocks.

Using a general linear model, this relationship was described with a high degree of precision (95.3% of variance described) using only calibration block thickness as the predictor (Model 2; Table 4**Error! Reference source not found.**). Of course the chemical fat % itself is likely

to affect the precision of this thickness estimate, hence it was not surprising that when it was also included in the prediction model (Model 1; **Error! Reference source not found.**), it did improve the precision of the estimate (99.9% of variance described). However this effect was particularly small relative to the importance of thickness itself.

Table 4: F-values and coefficients for the prediction of thickness from the log(pixel value) of the low energy image (Model 2), and using log(pixel value) of the low energy image and Chemical Lean % (Model 1).

	Thickness			
	Model 1		Model 2	
Parameter	*F value*	*Coeff±SE*	*F value*	*Coeff±SE*
Intercept		468.6±3.340		*416.4±12.593*
Ln(low energy)	10565.2*	-52.74±0.513	*563.6***	*-47.23±1.989*
Chemical Lean%	170.0*	-0.64±0.049		
*Ln(LE) * Lean%*	49.92*	0.05±0.007		
R-Square		0.999		*0.953*
RMSE		1.013		*9.008*

*, P<0.01; Thickness = tissue thickness (mm).

From these findings, it appears that the existing Automated Beef Rib Cutting x-ray system is suitable for producing R-values that can be used to determine the proportions of fat and lean within the soft-tissue pixels. However, these R values are impacted by tissue depth, necessitating correction particularly to enable an accurate estimation of the proportion of fat and lean within the soft-tissue pixels. This correction can be provided by the log(pixel value) from the low energy image to estimate depth and volume. Thus the combination of log(pixel value) and pixel R Value should be able to estimate the fat and lean composition of soft-tissue pixels.

The key concern with the existing DEXA prototype is that tissue depths of 10 mm or less (and possibly higher) are not detected within the low energy image. This will limit the capacity for this system to predict carcass composition, given that the greater sensitivity to differentiating fat from lean tissue is found at the smallest tissue depths.

4.2 DEXA and CT scanning of six beef sides

Descriptive statistics of the carcases scanned within batch 1, and 2 are shown in

Table 5 below. The intention was to scan carcasses across a diverse range of weight and fatness (selected based upon P8 fat depths). As can be seen, one carcass was particularly lean (carcase 5: P8 = 1mm; CT fat % = 10.2%), and one carcass was particularly fat (carcase 6: P8 = 20mm; CT fat % = 24%).

Table 5: Descriptive statistic on the beef sides scanned

Carcase Number	*Works Number*	*Grade*	*Weight*	*P8mm*	*CTLean%*	*CTFat%*	*CTBone%*
1	397L	YH	140.5	9	63.66	20.73	15.61
2	516R	GD	168	8	64.78	18.61	16.60
3	521L	GD	146.5	10	62.41	19.74	17.86
4	395L	F	143.5	4	65.58	16.69	17.73
5	400R	F	110.5	1	69.36	10.17	20.47
6	406R	N	152.5	20	58.03	23.79	18.17

The first phase in this process is to remove bone containing pixels on the basis of thresholding those pixels with values above the mean. The effectiveness of this is evident within Figure 13 below where pixels associated with the ribs, forelimb and spinal column have been removed as well as pixels from area's around the spine and forequarter where tissue depths are particularly high.

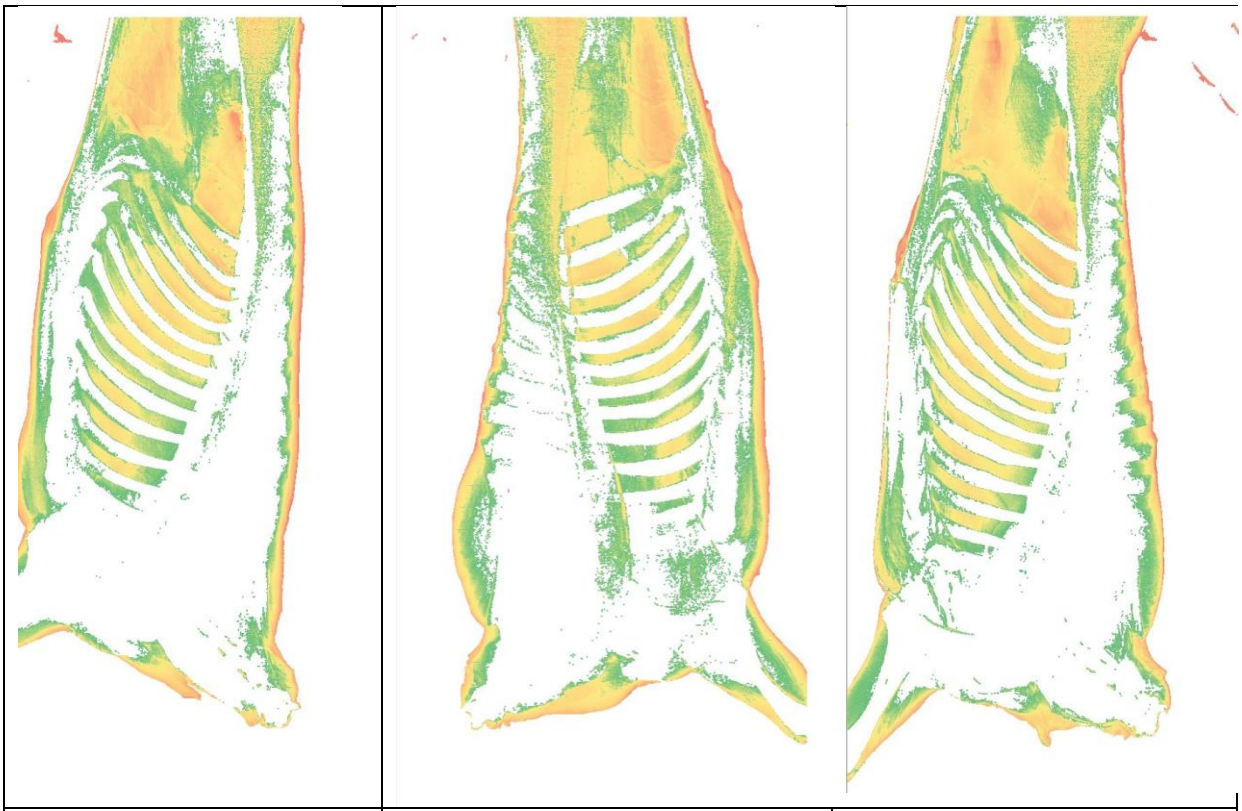

Carcase 1	**Carcase 2**	**Carcase 3**

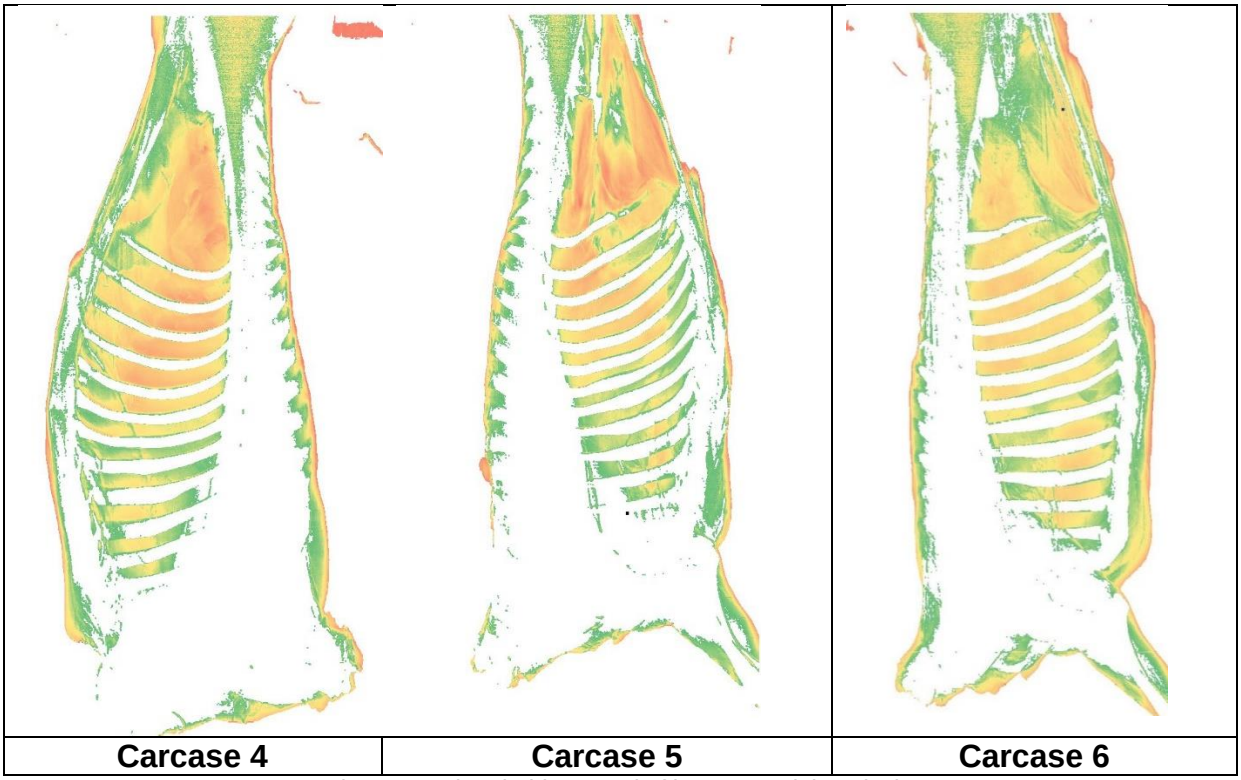

Figure 13: Threshold removal of bone-containing pixels.

However, initial assessment of the association between DEXAlean value and estimates of CTLean%, CTFat%, and CTBone% demonstrated no obvious relationship (see Figure 14, Figure 15; Figure 16). While carcases 6, 1, 3, and 2 do appear to have been ranked correctly on the basis of their CTFat% (see Figure 15), carcases 4 and 5 are quite divergent to this relationship.

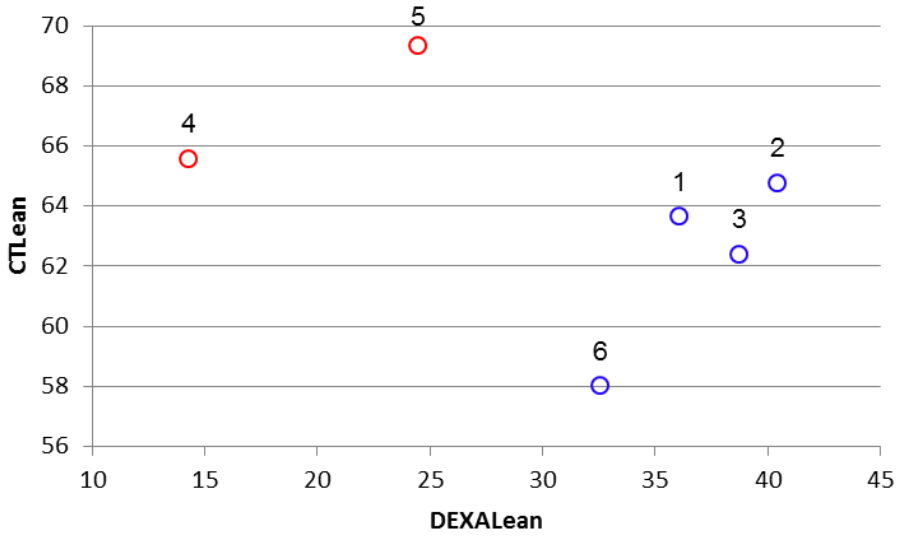

Figure 14: Relationship between CT Lean % and DEXALean value.

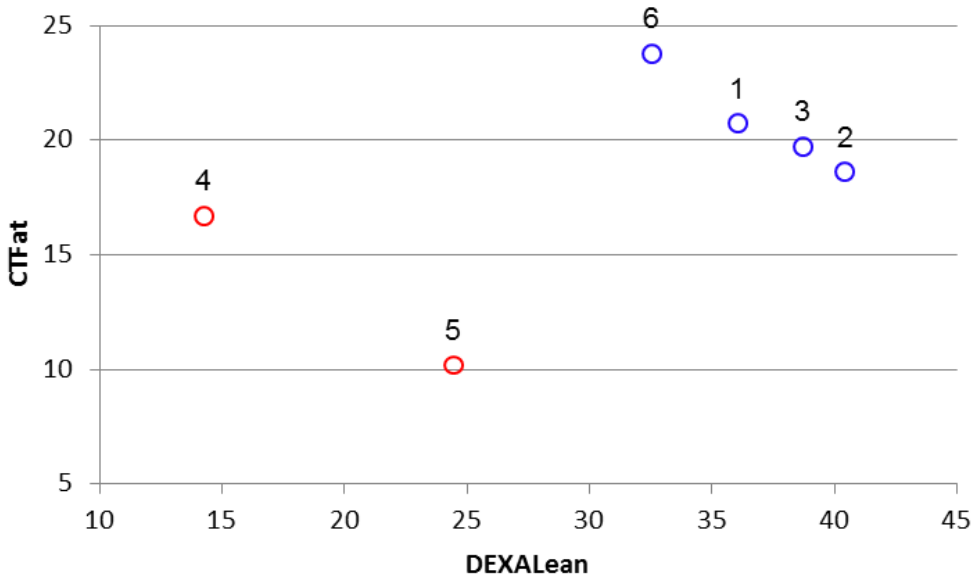

Figure 15: Relationship between CT Fat % and DEXALean value.

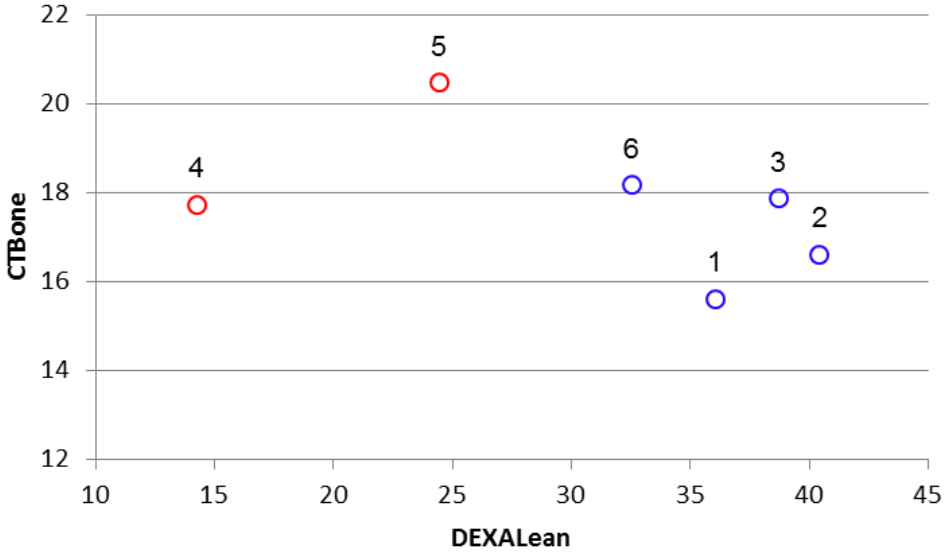

Figure 16: Relationship between CT Bone % and DEXALean value.

In an attempt to explore these results in more detail, it was decided to focus upon the association between DEXA value and CT Fat% as previous estimates of body composition have been most successful for predicting CT Fat%. On this basis two carcases (carcases 4 and 5 which are highlighted in red) are clear outliers from the rest of the observations (see Figure 15). Frequency plots for the pixels within these images demonstrate a bi-modal distribution, with an apparent small secondary peak at R values of about 0.8 (see Figure 17).

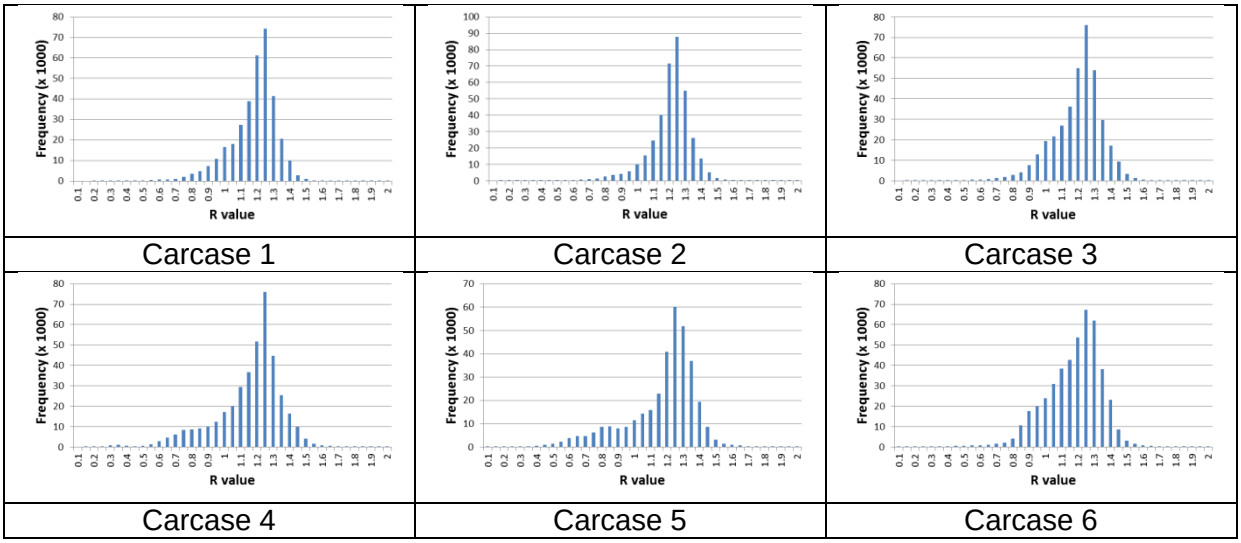

Figure 17: Frequency distributions of R values for each carcase image.

To explore the relevance of this bi-modal distribution, a second threshold was applied to the distribution, removing pixels with values above the mean for each image, as well as below an arbitrarily assigned second threshold value of 0.9. The resulting frequency distributions are shown in Figure 18. This approach has still resulted in adequate removal of bone containing pixels within each image, as shown in Figure 19 below.

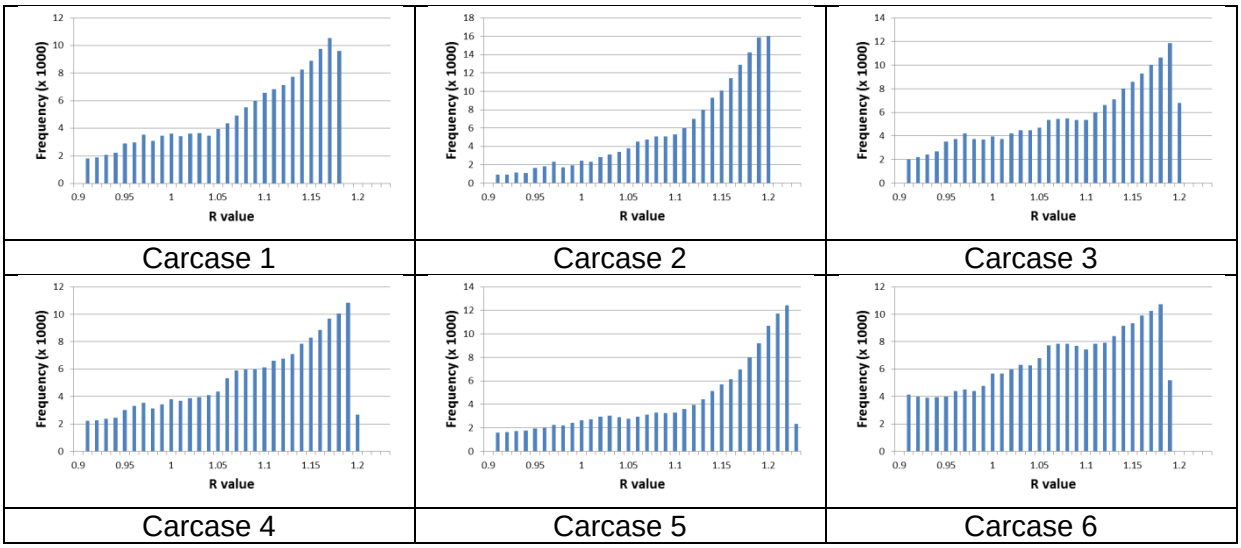

Figure 18: Frequency distributions of R values for each carcase image after threshold removal of pixel values above the mean, and below an R value of 0.9.

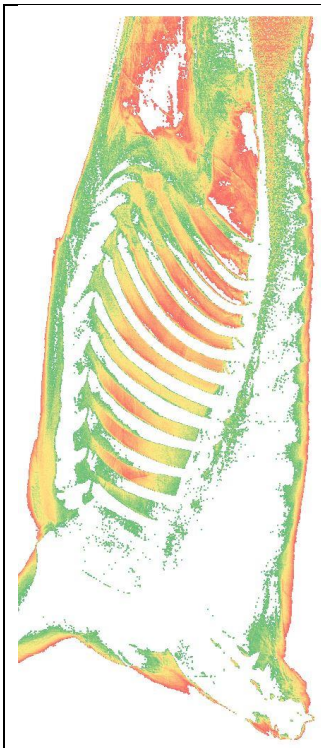	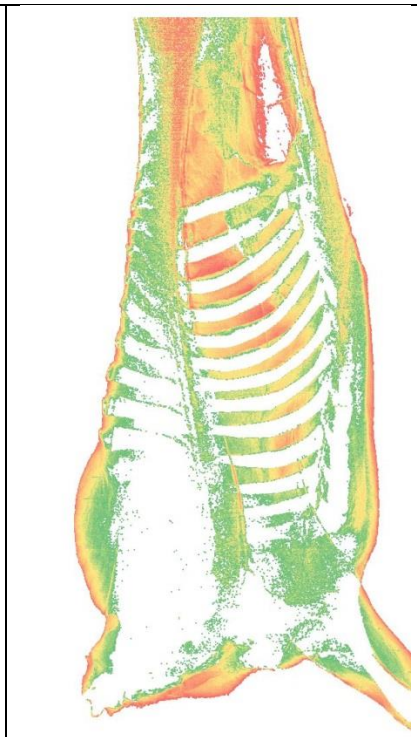	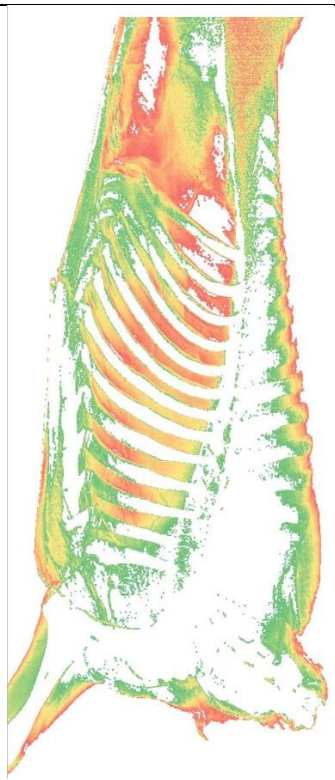
Carcase 1	**Carcase 2**	**Carcase 3**
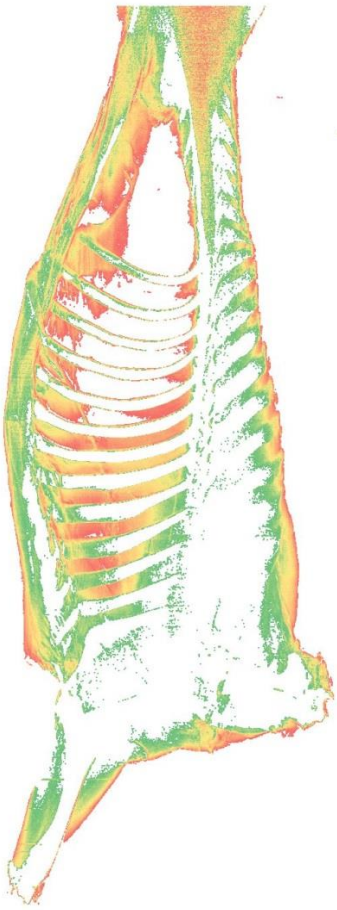	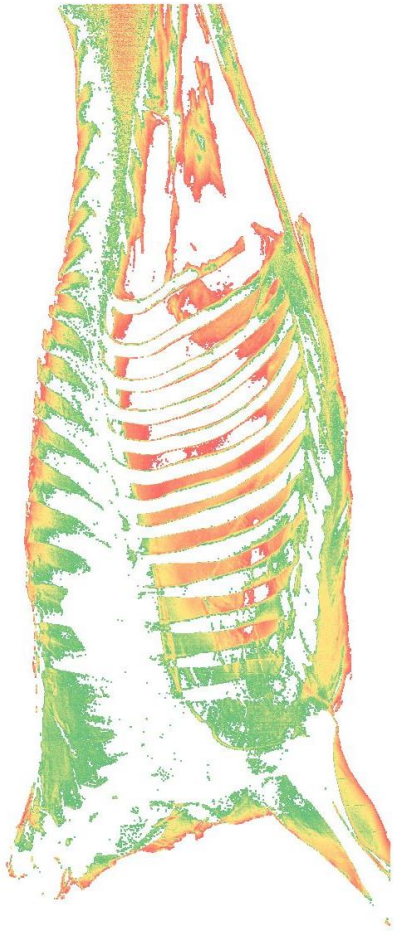	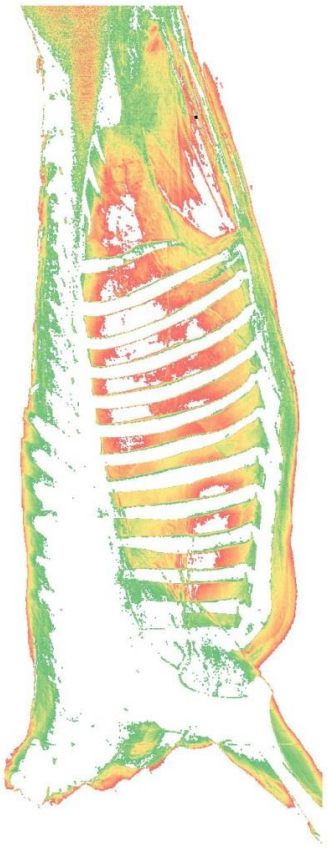
Carcase 4	**Carcase 5**	**Carcase 6**

Figure 19: Carcase images after threshold removal of pixels with values above the mean, and below an R value of 0.9.

The resulting association between DEXAlean value and estimates of CTLean%, CTFat%, and CTBone% were somewhat improved (see Figure 20, Figure 21, Figure 22), in particular with appropriate differentiation between carcase 5 and carcase 6 on the basis of fat and lean content. While this re-working of the images is quite arbitrary, and therefore not a commercially relevant solution, it does suggest that there is some potential for determining carcase composition. Nonetheless it doesn't identify the reasons for the divergent DEXA values for carcases 4 and 5. Some ideas for these divergent results may be:

1. Inconsistent scanning of carcase sections. Given the way in which imaging is carried out, carcases of variable size will intersect the top of the scanning region at variable positions, and therefore have varying proportions of the carcase imaged. However while carcase 5 was the smallest, carcase 4 was simply in the middle of the weight range, making this suggestion less likely.
2. Loss of 10mm tissue depths. As discussed previously, this is likely to have removed important regions around the outside surface of the images, resulting in the loss of important regions for predicting carcase composition.
3. Changed scanning parameters or other inconsistencies in image acquisition. This seems less likely as the system is automated and was calibrated at the start of the scanning run. None-the-less, if there were altered scanning parameters for carcases 4 and 5 it would explain their divergent results.

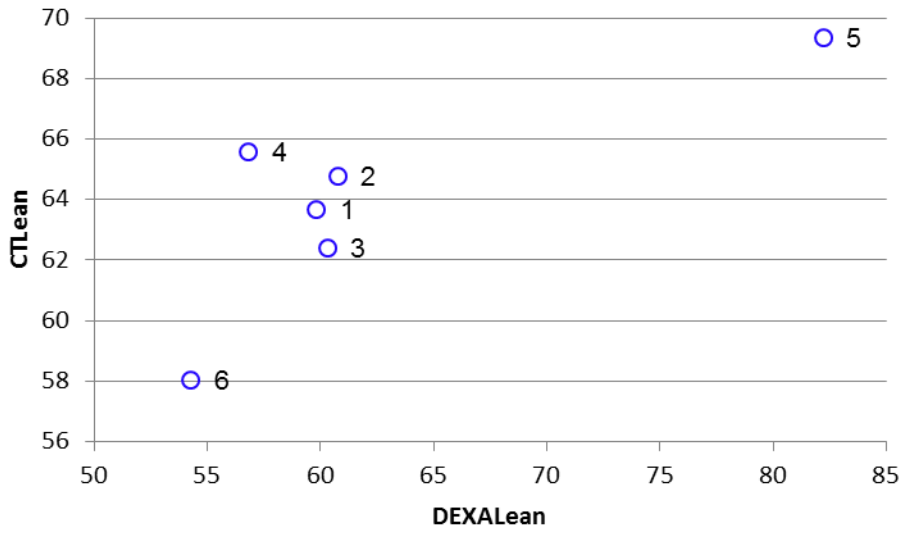

Figure 20: Relationship between CT Lean % and DEXALean value after including an additional threshold, removing pixels with an R value below 0.9.

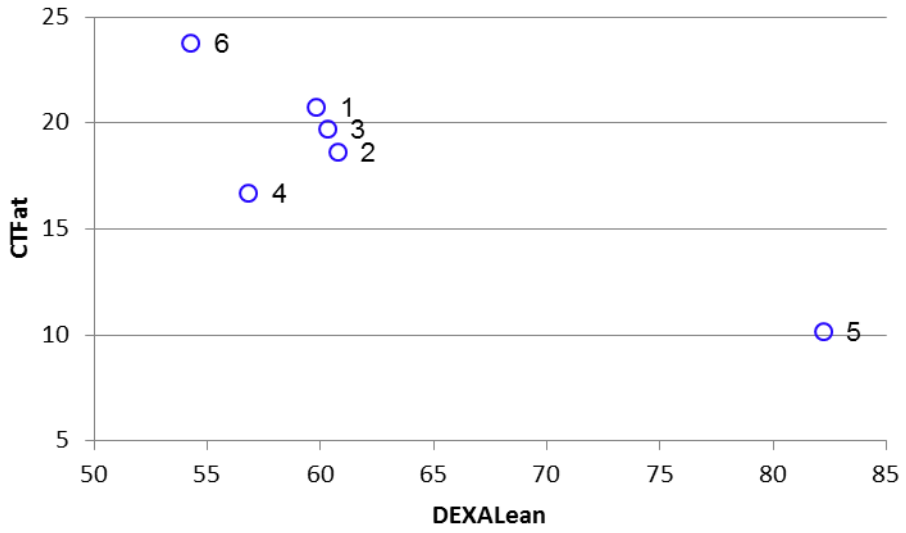

Figure 21: Relationship between CT Fat % and DEXALean value after including an additional threshold, removing pixels with an R value below 0.9.

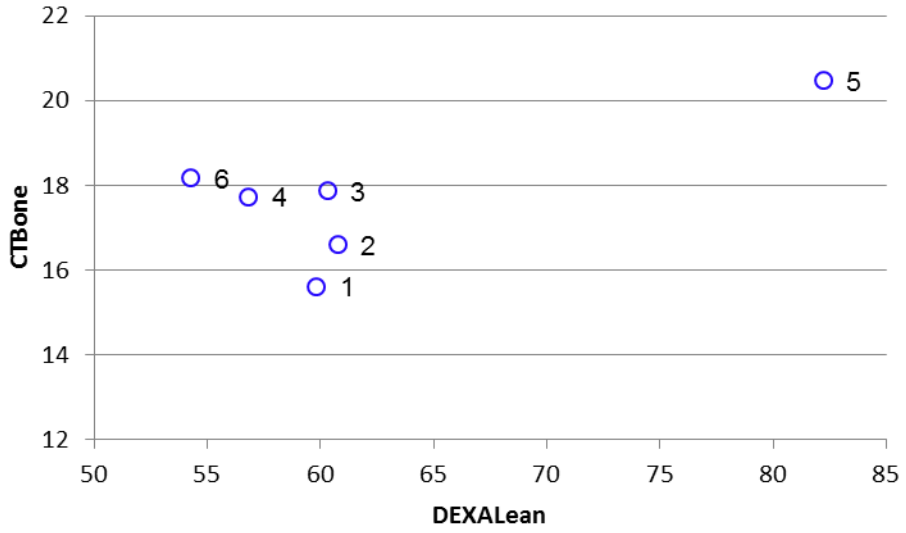

Figure 22: Relationship between CT Bone % and DEXALean value after including an additional threshold, removing pixels with an R value below 0.9.

The Rib Cutter's DEXA system demonstrates good potential for predicting fat:lean ratio's in tissue depths of 80 – 160mm. However, tissue depths of 10mm are not detected at low energy levels, and presumably at depths greater than this depth but less than 80mm. This deficiency needs to be addressed as previous work in lamb has indicated that significant prediction power is derived from these shallow tissue depths. This may well be the cause of the poor differentiation of fat and lean carcases within the subsequent carcase scans.

4.3 Second set of phantom and carcase scans at production X-Ray levels and reduced X-Ray levels.

Following the results obtained from the initial six carcases, another set of trials was then performed. The tissue phantom was again scanned and analysed along with eight carcases.

4.3.1 Tissue Phantom Analysis

As before, there was a negative linear relationship between increasing chemical fat % and the corresponding average R value for the 10mm, 80 mm and 160 mm tissue phantoms (Figure 23) although that the DEXA system loses sensitivity for determining fat:lean composition when passing through tissues of greater depth.

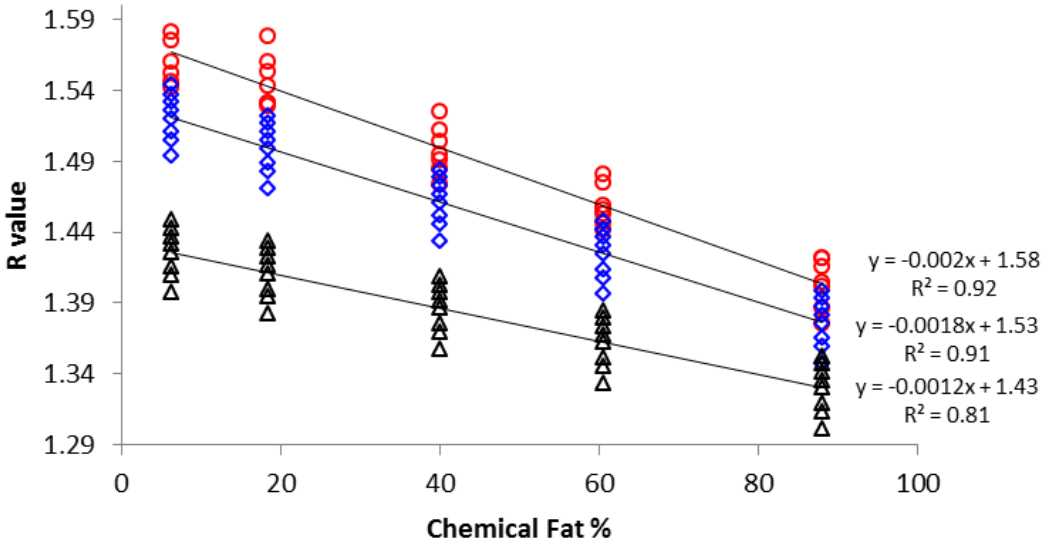

Figure 23: Relationship between R value and chemical fat % in tissue calibration blocks of 12.5mm (O), 80mm (◇), and 160mm (Δ).

As per the first trials, when this relationship is inverted and a general linear model is used to describe Chemical Fat %, it has a high degree of precision (94% of variance described), with the coefficients as shown in

Table 6. This implies that we can solve for Chemical Fat % but must have knowledge of both R-values and tissue thickness.

A key finding in this set of trials was the effect of pixel height within each image, with R-values diminishing across the height of the detector. Inversely this is evidenced as a positive coefficient in

Table 6 below. This height adjustment had no effect on the other coefficients within

Table 6, however it does improve the residuals of the relationship, as can be seen within Figure 24.

Table 6: F-values and coefficients for the prediction of chemical Fat% using average R-value and thickness of calibration blocks.

	Percent Lean	
	F value	*Coefficient±S.E.*
Intercept		*787.4±27.75*
R value	*729**	*-506.2±18.74*
Thickness	*10.69**	*0.9±0.28*
*R value*Thickness*	*25.36**	*-0.99±0.196*
Height	*200**	*0.04±0.003*
R-Square		*0.94*
RMSE		*7.167*

*, P<0.01; Thickness = tissue thickness (mm); RMSE, Root Mean Square Error.

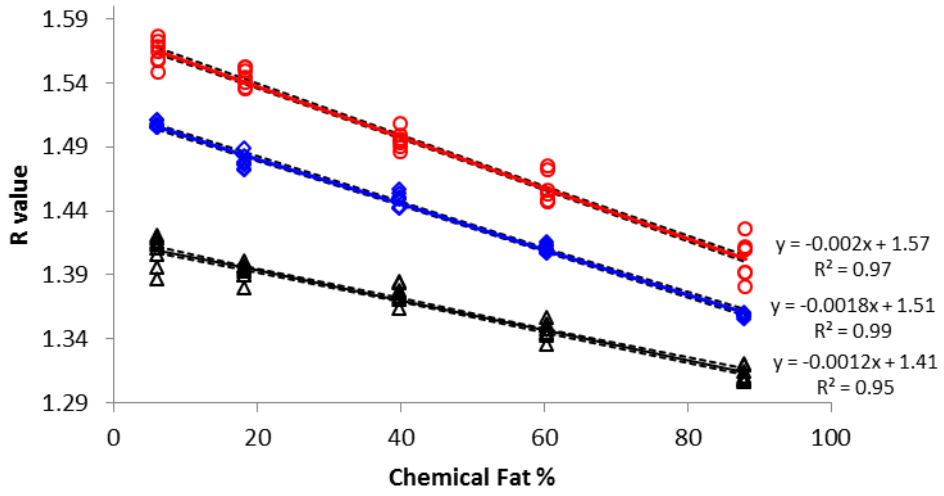

Figure 24: Relationship between R value and chemical fat % in tissue calibration blocks of 12.5mm (O), 80mm (◇), and 160mm (Δ) after pixel height adjustment.

Using this correction, the potential for determining tissue thickness by using the log(pixel value) from the low energy image was re-investigated. When assessed graphically, the relationship between tissue thickness and log(pixel value) demonstrated a linear trend (**Error! Reference source not found.**), with the 160mm calibration blocks having log(pixel values) approximately 3.5 units lower than the 12.5mm calibration blocks.

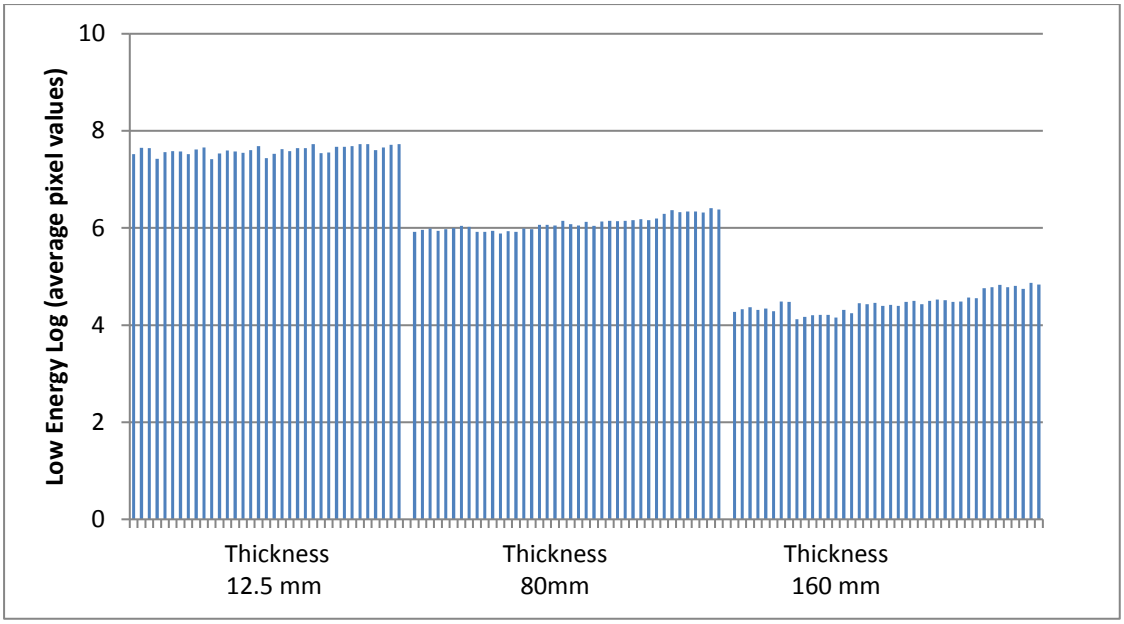

Figure 25: Log(average pixel value) from the low energy image for each of the calibration blocks.

Using a general linear model, this relationship was described with a high degree of precision (98% of variance described) using only calibration-block thickness as the predictor (Model 2; **Error! Reference source not found.**). Of course the chemical fat % itself is likely to affect the precision of this thickness estimate, hence it was not surprising that when it was also included in the prediction model (Model 1; **Error! Reference source not found.**), it did improve the precision of the estimate (99.9% of variance described). However this affect was particularly small relative to the importance of thickness itself. This represented a significant improvement over the initial phantom trial results, demonstrating the importance of correcting for this height effect.

Table 7: F-values and coefficients for the prediction of thickness from the log(pixel value) of the low energy image (Model 2), and using log(pixel value) of the low energy image and Chemical Lean % (Model 1).

	Thickness			
	Model 1		Model 2	
Parameter	*F value*	*Coeff±SE*	*F value*	*Coeff±SE*
Intercept		*343.8±3.015*		*365.4±3.345*
Ln(low energy)	*7923**	*-44.3±0.498*	*7234**	*-46.5±0.546*
Chemical Fat%	*92.0**	*0.60±0.062*		
*Ln(LE) * Chemical Fat%*	*42.2**	*-0.07±0.010*		
R-Square		*0.999*		*0.98*
RMSE		*3.934*		*7.488*

*, P<0.01; Thickness = tissue thickness (mm).

4.3.2 Carcase Data Analysis (8 sides)

Descriptive statistics of the carcases scanned are shown in Table 8Error! Reference source not found. below. The intention was to scan carcasses across a diverse range of weight and fatness (selected based upon P8 fat depths).

Table 8: Descriptive statistics for key traits. Values are mean ± standard deviation (min, max).

	Full composite Carcase
P8 fat	10.62± 4.53 (5 , 18)
Cold weight at DEXA	122.50± 9.02 (112.5 , 136.0)
CT Lean %	68.23± 2.85 (64.2 , 72.2)
CT Fat %	15.18± 3.62 (12.0 , 21.1)
CT Bone %	16.59± 2.12 (13.5 , 19.6)
DEXA Value (height adjustment)	83.31± 7.63 (73.3 , 95.9)
DEXA Value (no height adjustment)	70.87± 8.33 (59.9 , 83.3)
13th rib forequarter DEXA Value (height adjustment)	85.49± 12.62 (64.84 , 99.41)

The first phase in the image analysis process is to remove bone containing pixels on the basis of thresholding those pixels with values above the mean. The effectiveness of this is evident within Figure 28 below**Error! Reference source not found.** where pixels associated with the ribs, forelimb and spinal column have been removed. The removal of bone-containing pixels from regions of greatest tissue depth (i.e. around the shoulder region) was less precise. This is likely to affect accuracy and precision for predicting composition in these regions.

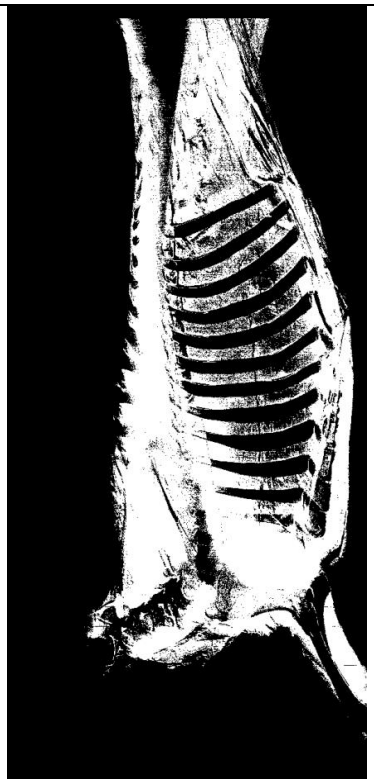

Carcase 1

CTFat = 11.95 CTLean = 70.08
CTBone = 17.98 CCWT = 115.5

Carcase 2

CTFat = 11.97 CTLean = 68.44
CTBone = 19.59 CCWT = 127

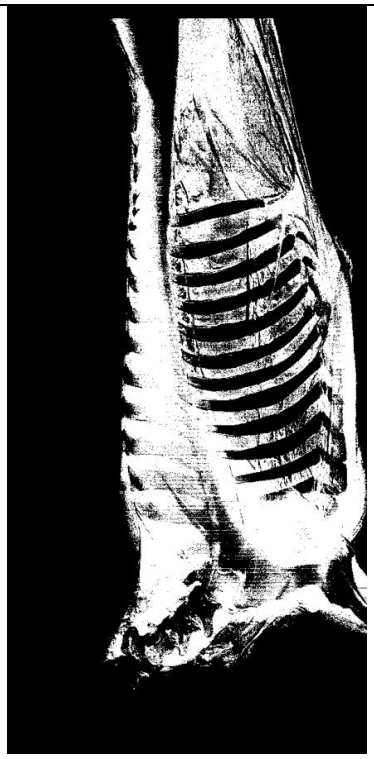

Carcase 3

CTFat = 13.05 CTLean = 69.19
CTBone = 17.77 CCWT = 136

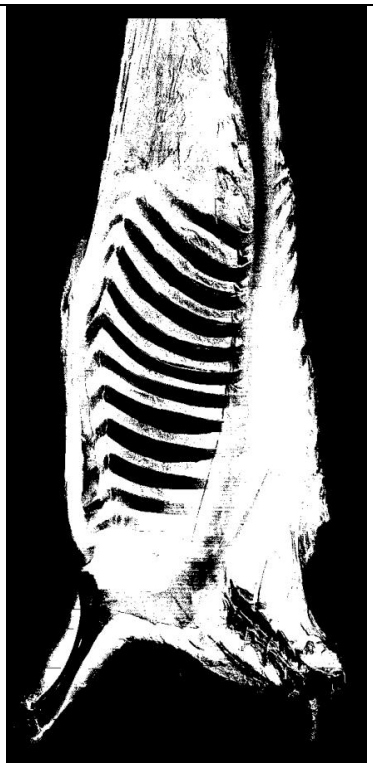

Carcase 4

CTFat = 17.72 CTLean = 64.16
CTBone = 18.12 CCWT = 129.5

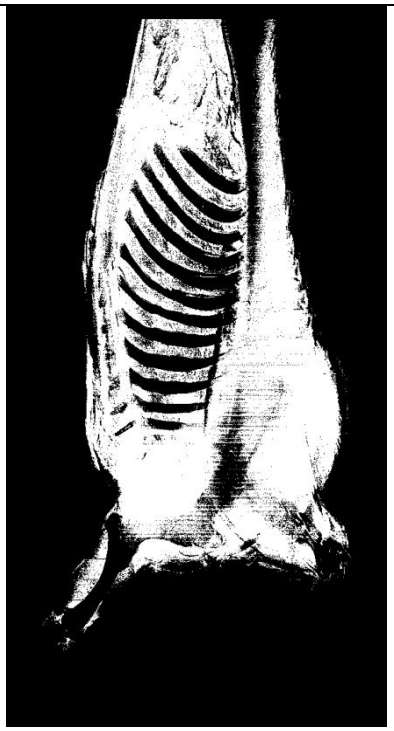 **Carcase 5**	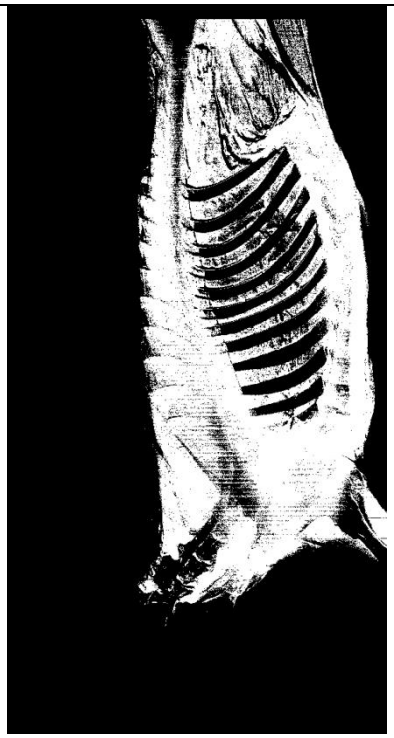 **Carcase 6**
CTFat = 19.29 CTLean = 67.2 CTBone = 13.46 CCWT = 117	CTFat = 13.45 CTLean = 70.27 CTBone = 16.28 CCWT = 113
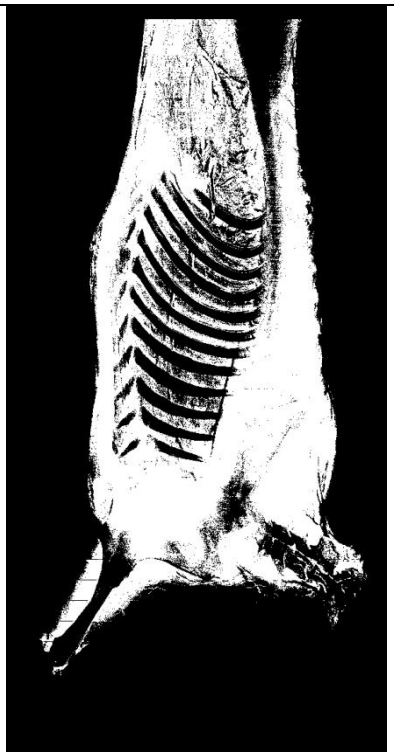 **Carcase 7**	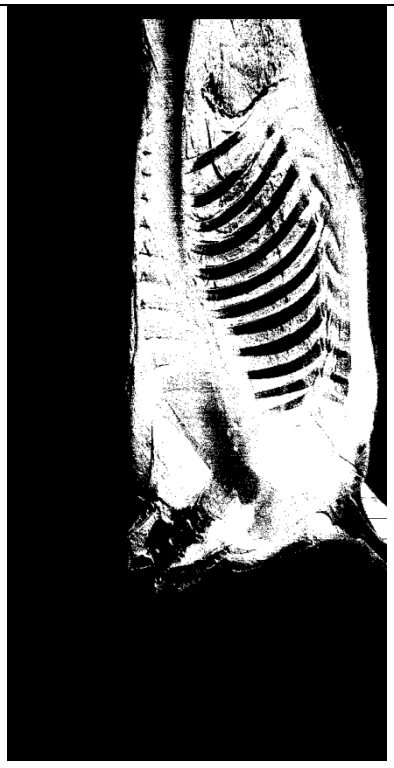 **Carcase 8**
CTFat = 12.94 CTLean = 72.16 CTBone = 14.90 CCWT = 112.5	CTFat = 21.10 CTLean = 64.30 CTBone = 14.60 CCWT = 129.5

Figure 26: Threshold removal of bone containing pixels from all carcases.

The prediction of CT composition varied between tissue types. The best results were those achieved for CT bone%. In this case the R^2 values were 0.75 for predicting CT bone% (**Error! Reference source not found.Error! Reference source not found.**), and as high as 0.82 when cold carcase weight was also included in the model (Figure 29; **Error! Reference source not found.**). The inclusion of the pixel height adjustment did not further improve this precision (**Error! Reference source not found.**). Alternatively, the DEXA value provided no significant prediction of CT lean% (Figure 27**Error! Reference source not found.**; **Error! Reference source not found.**) or CT fat% (Figure 28**Error! Reference source not found.**; **Error! Reference source not found.**), irrespective of whether the image analysis incorporated a pixel height adjustment.

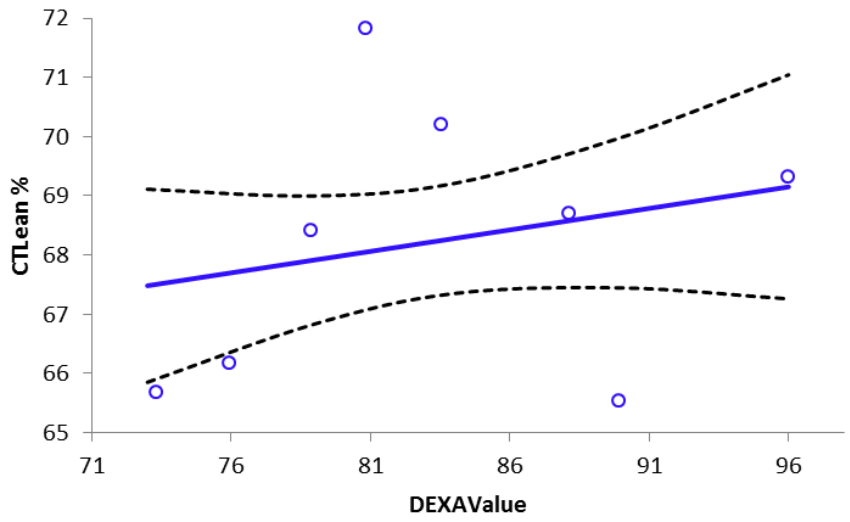

Figure 27: Association between CT lean% and DEXA Value adjusted for the nylon phantom, within a model also containing cold carcase weight. Icons represent raw data, and lines are predicted means (±SE).

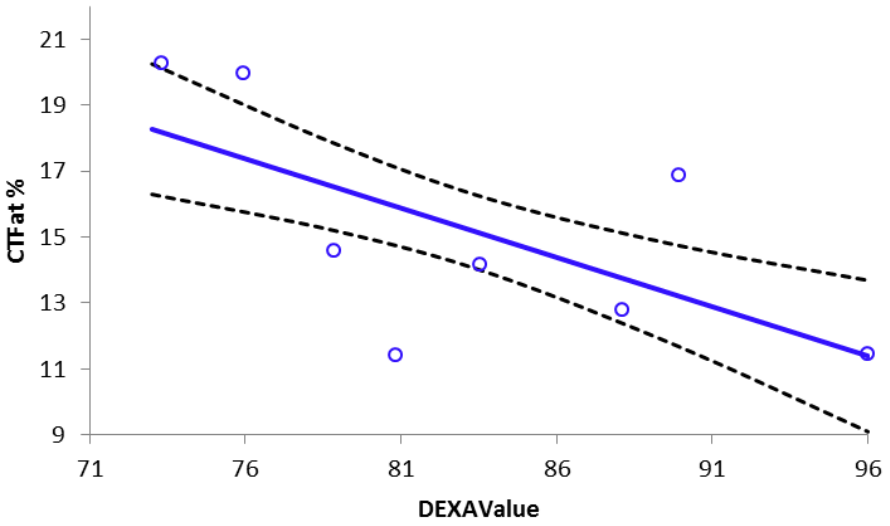

Figure 28: Association between CT fat% and DEXA Value adjusted for the nylon phantom, within a model also containing cold carcase weight. Icons represent raw data, and lines are predicted means (±SE).

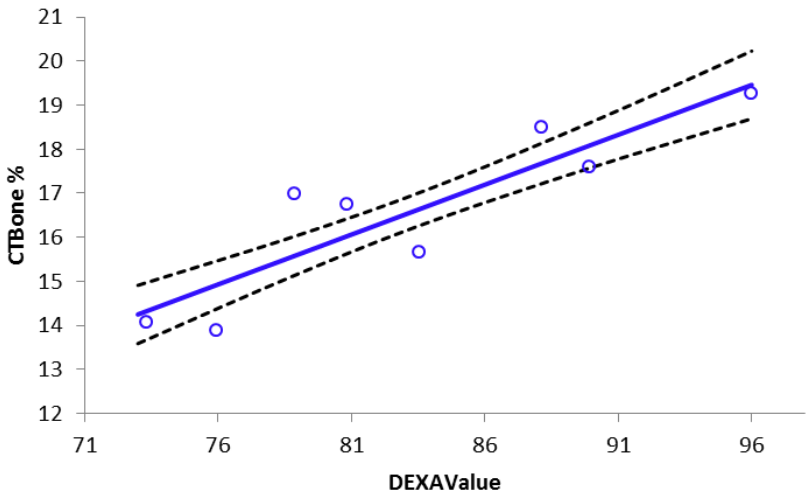

Figure 29: Association between CT bone% and DEXA Value adjusted for the nylon phantom, within a model also containing cold carcase weight. Icons represent raw data, and lines are predicted means (±SE).

These analyses were repeated after editing images to remove the image section distal to the 13th rib, manually optimising image alignment to best match pixels, and incorporating the height effect, and this had a substantial impact on precision. Again the best results were those achieved for CT bone% with R^2 values of 0.78 for predicting CT bone% (

Table 9), and as high as 0.93 when cold carcase weight was also included in the model (Figure 32; **Error! Reference source not found.**). Importantly, there was a strong association between DEXA value and CT fat % with R^2 values of 0.71 for predicting CT fat% (

Table 9), and as high as 0.78 when cold carcase weight was also included in the model (Figure 31;

Table 9). As with the other analyses DEXA value did not predict CT lean% (Figure 30; Table 9).

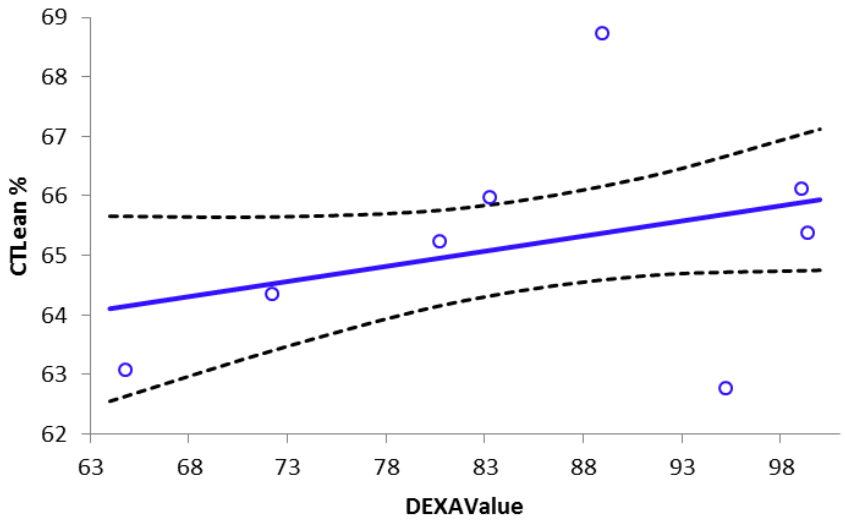

Figure 30: Association between CT lean% and DEXA value after adjusting images based on their nylon phantom value, pixel height, and truncating the images to remove that section distal to the 13th rib. This value was fitted within a model also containing cold carcase weight. Icons represent raw data, and lines are predicted means (±SE).

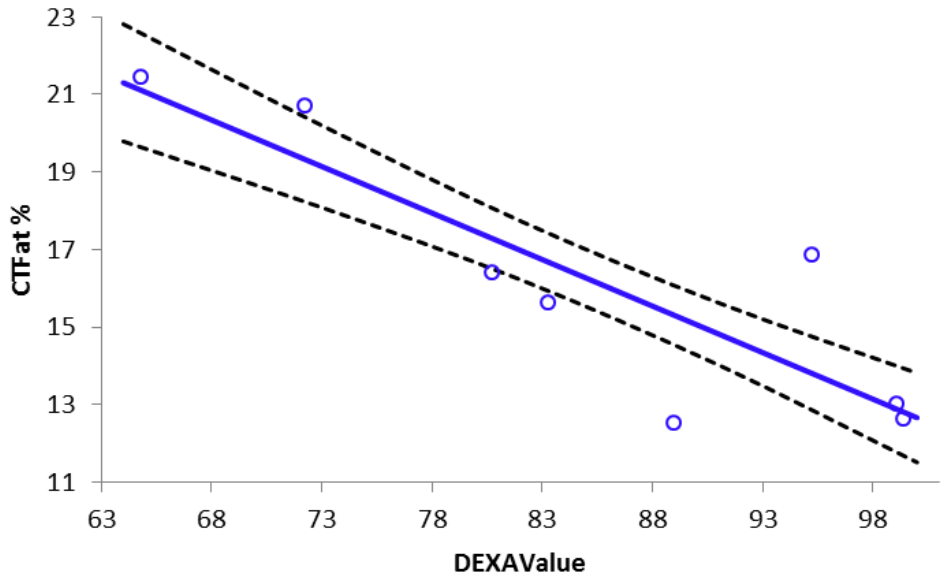

Figure 31: Association between CT fat% and DEXA Value after adjusting images based on their nylon phantom value, pixel height, and truncating the images to remove that section distal to the 13th rib. This value was fitted within a model also containing cold carcase weight. Icons represent raw data, and lines are predicted means (±SE).

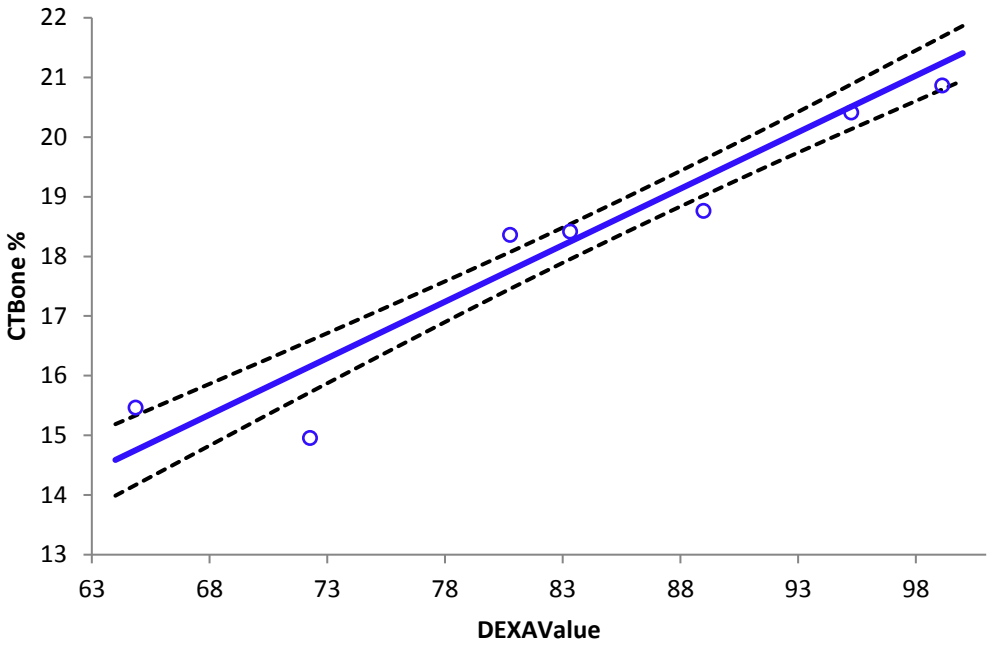

Figure 32: Association between CT bone% and DEXA value after adjusting images based on their nylon phantom value, pixel height, and truncating the images to remove that section distal to the 13th rib. This value was fitted within a model also containing cold carcase weight. Icons represent raw data, and lines are predicted means (±SE).

Table 9: Models predicting CT Lean, Fat and Bone %. CT composition was predicted using adjusted DEXA values which were normalised to a fixed value for the nylon phantom scanned in each image (DEXA value), and then with the additional inclusion of cold carcase weight in these models (DEXA Value inc. CCWT). These models were derived for data without adjusting for pixel height in the image analysis phase, then with this height adjustment, and then finally with height adjustment and forequarter image-section only. F-value, intercept and coefficients are reported for each model, as well as estimates of precision (R^2, root-mean-square-error (RMSE)).

		Full image No height adjustment		Full image With Height Adjustment		Forequarter only With Height Adjustment	
		DEXA Value	DEXAValue inc CCWT	DEXA Value	DEXAValue inc CCWT	DEXA Value	DEXAValue inc CCWT
CT Lean%	F Value CCWT		3.28		3.18		6.10
	F Value DEXAValue	0.04	0.32	0.11	0.31	0.57	0.64
	Intercept	66.29	88.14	64.06	86.21	59.64	86.25
	CCWT		-0.20		-0.20		-0.39
	DEXAValue	0.03	0.07	0.05	0.07	0.07	0.05
	R2	0.01	0.40	0.02	0.40	0.09	0.59
	RMSE	3.071	2.614	3.053	2.615	2.870	2.111
CT Fat%	F Value CCWT		1.13		0.82		1.53
	F Value DEXAValue	2.94	3.62	3.40	3.59	14.84**	15.13*
	Intercept	32.85	17.28	38.96	25.31	37.25	24.29
	CCWT		0.14		0.12		0.19
	DEXAValue	-0.25	-0.28	-0.29	-0.30	-0.25	-0.24
	R2	0.33	0.45	0.36	0.45	0.71	0.78

	RMSE	3.203	3.168	3.124	3.172	2.140	2.051
CT Bone%	F Value CCWT		1.65		2.84		10.80*
	F Value DEXAValue	19.16**	18.42**	15.31**	18.39**	21.21**	59.91**
	Intercept	0.87	-5.43	-3.02	-11.52	3.09	-10.56
	CCWT		0.06		0.08		0.20
	DEXAValue	0.22	0.21	0.24	0.23	0.18	0.19
	R2	0.76	0.82	0.72	0.82	0.78	0.93
	RMSE	1.117	1.061	1.214	1.062	1.320	0.814

* P< 0.05; **, P< 0.01.

5 Conclusions/Recommendations

It appears that the existing Automated Rib Cutting DEXA system is suitable for producing R-values that can be used to determine the proportions of fat and lean within the soft-tissue pixels. However, these R-values are impacted by pixel height within the image and tissue depth, necessitating correction particularly to enable an accurate estimation of the proportion of fat and lean within the soft-tissue pixels. The thickness correction can be provided by the log(pixel value) from the low energy image to estimate depth and volume, and the height correction modelled simply as a linear adjustment to the R-values. Thus the combination of pixel R-value corrected for height within the image, as well as log(pixel value) to reflect pixel thickness and therefore volume should be able to estimate the fat and lean composition of soft-tissue pixels.

The DEXA system demonstrated a high level of precision for predicting bone composition in the fore section of beef carcases. This may be associated with variability in the effectiveness of threshold removal of bone-containing pixels, creating a continuum in the remaining pixels that correlates with the proportions of carcase bone. This was significantly enhanced by truncating the DEXA image to exclude that section distal to the 13th rib and aligning the images more precisely. The DEXA system also demonstrated a good prediction of CT fat%, but only in the analysis where the images were truncated and aligned. This improvement associated with image truncation and pixel alignment is likely due to two factors. Firstly, pixel alignment is essential for calculating the attenuation ratio values which are fundamental to this method. Previous work in lamb has demonstrated that when the high and low energy

DEXA images were mismatched by just one pixel, this offset the accuracy of the R-values, severely eroding their precision for predicting carcase composition. A mismatch of two pixels completely removed any predictive power. This would be particularly important in “non-homogenous” carcase tissue, yet far less important in the “highly-homogenous” tissue phantoms, explaining the excellent results achieved in part one of this report which detailed the prediction of these phantoms. Secondly, truncating the DEXA image would have improved the consistency of the proportion of the carcase that is captured by the DEXA scan, which is likely to have improved the association between DEXA value and whole carcase composition.

At this point there is still no significant association between DEXA value and lean tissue proportion. This contrasts with earlier studies in lamb where CT lean% was predicted, albeit with less precision. One possible reason for this may be associated with variation in the large portion of lean tissue within the hind-quarter of the carcase which is not visualised by the DEXA system. This highlights the need for more research to enable scanning of the hind-quarter using this DEXA system.

In conclusion, these results demonstrate that the DEXA hardware used in the beef automated rib cutting system could be a viable option for predicting beef carcase composition in the fore-quarter section. The next step in this work would be to build on this data set, test its repeatability, and to test “within plant” factors that may impact on composition estimates.